AIAA Aviation
16-20 June 2014, Atlanta, GA
32nd AIAA Applied Aerodynamics Conference

2014-2151

Reynolds Number Effects on the Performance of Small-Scale Propellers

Robert W. Deters,* Gavin K. Ananda,† and Michael S. Selig‡

Department of Aerospace Engineering, University of Illinois at Urbana-Champaign, Urbana, IL 61801, USA

The growing use of small UAVs and MAVs has increased the interest in determining the performance of small-scale propellers that power them. These small-scale propellers operate at much lower Reynolds numbers than propellers for larger aircraft; typical Reynolds numbers for small-scale propellers are less than 100,000 based on the velocity and chord at the 75% span station. The low Reynolds numbers of the propellers make predicting the performance of these propellers difficult as the performance of the propellers generally change with Reynolds numbers. In order to understand the Reynolds number effects on small-scale propellers, the performance data of twenty-seven off-the-shelf propellers and four 3D-printed propellers were measured in both static and advancing-flow conditions. The diameters of these propellers ranged from 2.25 in to 9 in. From these tests, the performance of the propellers was shown to improve as the Reynolds number increased. This improvement was seen as either an increase in the thrust coefficient, a decrease in the power coefficient, or both. For propellers in an advancing flow, performance improvement was also seen as an increase in the propeller efficiency. Results from some of the propellers tested showed an efficiency improvement of around 10%. Nevertheless, the maximum efficiency achieved by the small-scale propellers is still low when compared to typical values of larger propellers.

I. Introduction

The number of small Unmanned Air Vehicles (UAVs) being designed and built is growing. Besides being a popular hobby in the form of remote-controlled (RC) aircraft, small UAVs are finding military and civilian applications. Many of these UAVs are fixed-wing aircraft and rotorcraft designed to carry small payloads and are mainly used for surveillance and reconnaissance. A subset of the small UAVs is the Micro Air Vehicles (MAVs), which have a maximum size of 6 in (15 cm). The small size of these aircraft leads to interesting and difficult aerodynamic concerns such as low Reynolds number effects.

Propellers provide the thrust for many of these small UAVs, and the small size of these propellers has them operating with Reynolds numbers typically less than 100,000. Airfoil testing at Reynolds numbers of 40,000 to 500,000 has shown that the lift decreases and the drag increases as the Reynolds number decreases with more pronounced effects at 100,000 and lower.[1–7] Since propeller thrust is largely dependent on the lift and power is largely dependent on the drag, the efficiency of a propeller is highly influenced by the Reynolds number.

The low Reynolds number effects can make predicting the performance of small-scale propellers difficult,[8–11] therefore a number of wind tunnel tests have been performed on small off-the-shelf propellers. Most of the current wind tunnel tests have been for propellers with a diameter of 6 in and larger,[10,12–17] with a few tests for propellers with a diameter of 5 in and smaller.[18–20] The main outcome from these propeller tests is that the Reynolds number of the propeller plays a significant part in determining its performance. The general trends are that as Reynolds number increases, the thrust increases, the power decreases, or both.

*Graduate Student, AIAA Student Member.
†Graduate Student, AIAA Student Member.
‡Associate Professor, AIAA Associate Fellow.

To help determine the effect of changing Reynolds numbers on the propeller performance, a testing rig was designed to measure the thrust and torque of propellers with diameters ranging from 2.25 in to 9 in. In total, the performance data of twenty-seven off-the-shelf propellers were measured in both static and advancing-flow conditions. Besides the off-the-shelf propellers, four propeller blades were designed and built using a 3D printer. A 5- and 9-in diameter version of each new propeller was built so that a large range of Reynolds numbers could be tested in both static and advancing-flow conditions. The 5-in propellers typically have a Reynolds number based on the chord at the 75% span location of less than 50,000, and the 9-in propellers have Reynolds numbers typically less than 100,000. The 5-in and 9-in propellers have an overlap Reynolds number region usually starting around a Reynolds number between 20,000 and 30,000.

II. Experimental Methodology

A. Equipment

Propeller tests were conducted in the UIUC low-turbulence subsonic wind tunnel. The wind tunnel is an open-return type with a 7.5:1 contraction ratio. The rectangular test section is 2.8×4.0 ft (0.853×1.22 m) in cross section and is 8 ft (2.44-m) in length. To account for the boundary-layer growth at the side wall, the width of the test section increases by approximately 0.5 in (1.27 cm) over the length of the test section. In order to have low turbulence levels at the test section, a 4-in (10.2-cm) honeycomb and four anti-turbulence screens are in the settling chamber. The resulting turbulence intensity for an empty tunnel has been measured to be less than 0.1% at all operating conditions.[21] A 125-hp (93.2-kW) AC motor driving a five-bladed fan is used to control the test-section speed up to 235 ft/s (71.6 m/s). The maximum test-section speed for these tests was 80 ft/s (24.4 m/s). Test-section speeds were measured using a MKS differential pressure transducer connected to static ports at the settling chamber and at the beginning of the test section. For test-section speeds below 40 ft/s, a MKS 220 1-torr transducer was used, and for speeds greater than 40 ft/s, a MKS 221 10-torr transducer was used. Ambient pressure was measured using a Setra Model 270 pressure transducer, and ambient temperature was measured using an Omega GTMQSS thermocouple.

Propeller performance was measured using the thrust and torque balance shown in Fig. 1. Thrust was measured outside of the tunnel test section using a T-shaped pendulum balance that pivoted about two flexural pivots and was constrained on one side by a load cell.[12] The Interface SMT S-Type load cell with a load capacity of 2.2 lb (9.8 N) was used for propellers with a diameter of 5.5 in (14.0 cm) and smaller, and the Interface SM S-Type load cell with a load capacity of 10 lb (44 N) was used for larger propellers. The balance was designed to allow the load cell to be placed in 10 different locations in order to use the full range of the load cell based on the thrust produced. The load cell locations ranged from 3.25 in (8.26 cm) from the pivot point to 7.75 in (19.69 cm) in 0.5-in (1.27-cm) increments. A preload weight was added to the balance on the opposite side to the load cell. This preload weight kept the load cell in tension during all aspects of testing to make sure the load cell would not slip during negative thrust conditions.

The torque from the propeller was measured using a reaction torque sensor (RTS) from Transducer Techniques. Propellers with a diameter of 5.5 in and smaller used a transducer with a capacity of 5 oz-in (0.0353 N-m) while 9-in propeller used a 25 oz-in (0.177 N-m) transducer. The torque cell was placed between the motor sting and the support arm of the thrust balance. To remove the torque cell, motor sting, balance support arm, and any wires from the propeller slipstream and test section velocity, a fairing surrounded the setup as shown in Fig. 2. The fairing spanned the test section from the floor to the ceiling in order to keep the test section flow symmetric. The NACA 0025 airfoil with a 24-in chord was used for the fairing to provide the necessary width required for torque sensor, motor sting, and all wires. The motor sting was long enough for all the propellers to be more than 1.5 diameters from the fairing in order to minimize the effect of the fairing on the propeller performance.

Propeller RPM was measured by shining a red laser with a wavelength of 630–680 nm through the propeller disc area to a phototransistor with a rise time of 5 μsec. The output from the phototransistor is amplified so that the maximum voltage when the laser shines on the receiver is over 2 V. As the propeller spins, the propeller blades block the laser beam, and the receiver output voltage drops to around zero. Each time the propeller RPM was measured, the voltage was recorded at 40,000 Hz for 30,000 samples. The high rate and sample number is used so that the resulting square wave is captured and the voltage peaks can be counted. The RPM was calculated by dividing the number of peaks by the sample time and by the number of propeller blades. The phototransistor rise time and the sample rate have been more than sufficient in

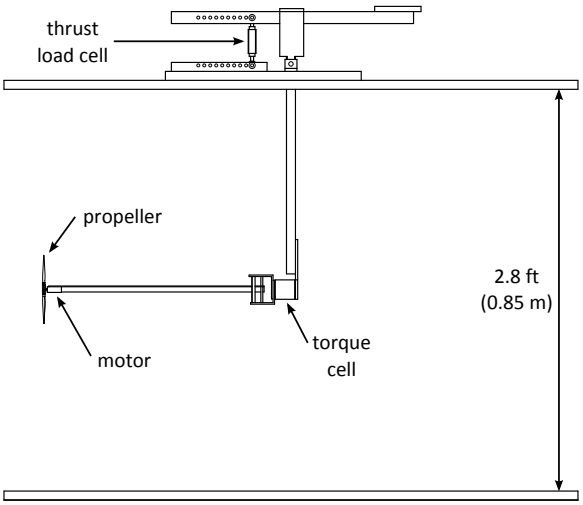

Figure 1: Propeller thrust and torque balance.

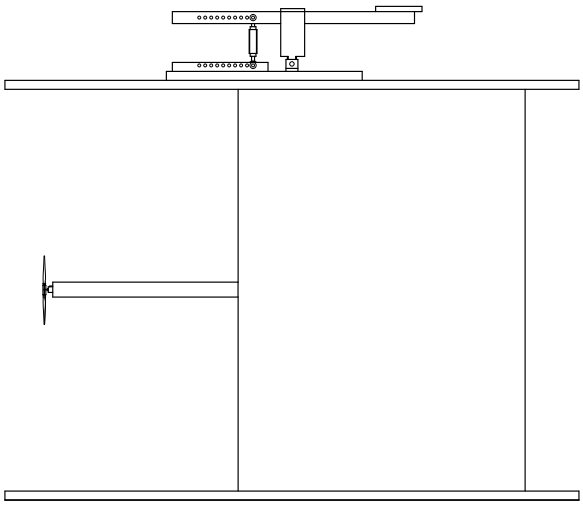

Figure 2: Propeller balance enclosed in fairing.

finding the typical RPM values for the propellers tested. This measurement technique was compared to results from a handheld digital tachometer, and the results agreed.

A variety of propellers were tested for this research. These propellers include off-the-shelf propellers from several manufacturers and some rapid-prototyped propellers. A discussion of the propellers is included in Section III. During the tests, the propellers with a diameter of less than 9-in were driven by the Medusa MR-012-030-4000 brushless motor using a Castle Creations Phoenix 10 speed controller. Propellers with a diameter of 9 in used an AstroFlight 803P Astro 020 Planetary System with a 4.4:1 gear ratio using a Castle Creations Phoenix 25 speed controller. To simplify the laboratory setup, a power supply by BK Precision was used to power the motor and speed controller. To set the rotational speed of the motor, the speed controller was connected to a modified ServoXciter EF from Vexa Control. While designed to test RC servos by adjusting the pulse-width signal to the servo, the ServoXciter also works well as the throttle for the motor. A voltage from the computer would be sent to the ServoXciter, and in turn the ServoXciter would then send a pulse-width signal to the speed controller to control the motor speed.

B. Testing Procedure

All voltages from the testing equipment were recorded by a National Instruments PCI-6031E 16-bit analog-to-digital data acquisition (DAQ) board connected to a personal computer. The DAQ board is capable of measuring 32 differential analog inputs simultaneously at a maximum sample rate of 100,000 samples/s. As mentioned earlier, propeller RPM measurements were recorded at 40,000 Hz for 30,000 samples. This high sample rate required the RPM measurement to be taken separately from the rest of the measurements. All other measurements (thrust, torque, tunnel pressures, atmospheric pressure, and temperature) were taken simultaneously immediately after the RPM measurement at a rate of 3,000 Hz for 3,000 samples. This method has been more than sufficient as differences in motor speed have been observed to change less than 1% during these time periods. A LabVIEW® program was written to read the DAQ board as well as control the motor speed and wind tunnel speed.

For static performance tests, the propeller thrust and torque were measured along with the ambient pressure and temperature at different RPM values. For advancing-flow performance tests, the propeller RPM was set and the tunnel speed was increased from 8 ft/s to 40 ft/s by 2 ft/s increments. During this test, a MKS 1-torr pressure transducer was used to measure the tunnel speed. At each velocity, the propeller thrust and torque were measured along with the tunnel speed and ambient pressure and temperature. If

the torque value became too close to zero, the test was stopped because the propeller was approaching the windmill brake state. If the propeller reached 40 ft/s before the windmill brake state was achieved, the same RPM was used for tunnel speeds of 34 ft/s to 80 ft/s by 2 ft/s increments using a MKS 10-torr transducer to measure the tunnel speed. Again the test would stop early if the propeller was close to windmilling. The overlap with the 1-torr and 10-torr tests were to ensure consistent data between low and high speed tests. Typically, at least three RPM values were tested to measure any Reynolds number effects.

C. Calibration

Since the DAQ board only records voltages from the transducers and load cells, each voltage is converted to a physical measurement through calibration curves. The pressure transducer that measured the ambient pressure and the thermocouple that measured ambient temperature used manufacturer supplied calibration equations to convert the voltages to pressure and temperature. The MKS differential pressure transducers used to measure tunnel pressures also used manufacturer calibration slopes.

The load and torque cells do not use manufacturer supplied calibration values. Instead, the calibration slopes are found during testing. Thrust calibration used precisely measured weights and a low-friction pulley system to create an applied axial load to simulate thrust on the load cell. By increasing and decreasing a known force on the load cell, a linear relationship between the thrust and voltage was determined. For torque calibration, the precision weights were used with a moment arm to create a known torque, and by adding and removing weights, a linear relationship between the torque and voltage was calculated. These calibration procedures were performed regularly to ensure consistent results, and any change in the slopes were typically 1% or less.

D. Data Reduction

As mentioned in Section A, the ambient pressure and temperature were measured using a pressure transducer and thermocouple, respectively. Air density was then calculated from the equation of state

$$p = \rho RT \tag{1}$$

where R is the universal gas constant. The standard value of 1716 $\text{ft}^2/\text{s}^2/^\circ\text{R}$ (287.0 $\text{m}^2/\text{s}^2/\text{K}$) for air was used.

Propeller power is calculated from the measured propeller torque by

$$P = 2\pi nQ \tag{2}$$

Performance of a propeller is typically given in terms of the thrust and power coefficients, defined as

$$C_T = \frac{T}{\rho n^2 D^4} \tag{3}$$

$$C_P = \frac{P}{\rho n^3 D^5} \tag{4}$$

where nD can be considered the reference velocity and D^2 can be considered the reference area. When the propeller is in a freestream flow, the advance ratio is defined in terms of the velocity and the rotation rate.

$$J = \frac{V}{nD} \tag{5}$$

By using the advance ratio, the thrust and power coefficients are now only a function of J, the Reynolds number, and the Mach number. The maximum Mach number for a propeller tip in these tests was about 0.26, which is below the incompressible limit. Therefore, compressibility effects were ignored, and the propeller performance is only a function of J and the Reynolds number. For this paper, the Reynolds number of a propeller was defined by the rotational speed and chord at the 75% blade station. The Reynolds number is defined as

$$Re = \frac{\rho V c}{\mu} \tag{6}$$

where the viscosity μ was calculated from Sutherland's formula.

The efficiency of a propeller is a measure of the useful power (TV) divided by the input power (P).

$$\eta = \frac{TV}{P} \tag{7}$$

Putting the efficiency in term of C_T, C_P, and J yields

$$\eta = \frac{C_T J}{C_P} \tag{8}$$

E. Wind Tunnel Corrections

Two wind tunnel corrections were used to account for the effects of testing a propeller in front of a fairing and in a closed test section. Since the propellers are tested on a string in front of a fairing, the air velocity seen by the propellers will be less than the velocity measured at the beginning of the test section. To account for this lower velocity, a velocity correction factor was developed based on the propeller size and its distance from the fairing.

Since the fairing spanned the test section from the floor to ceiling, the fairing was modeled as an airfoil using source panels. In order to satisfy the boundary condition of no cross flow at the tunnel side walls, reflections of the airfoil were included. The strength of each source panel and the flowfield surrounding the airfoil was then calculated using the method described in Anderson.[22] Using 100 sets of reflection pairs, the cross flow at the tunnel side walls was found to be less than $2 \times 10^{-6}\%$ of the freestream. The resulting 2D flowfield from the source panels was assumed to be the same along the span of the fairing. The propeller size is small compared with the height of the tunnel, so any wall effects from the floor and ceiling were assumed to be negligible. Since the propeller will see different corrected velocities along its disk area, a weighted average was used to calculate a single velocity reduction factor $k_{fairing}$ (Eq. 9). In order to simplify the calculations needed during testing, a series of correction factors were tabulated beforehand covering the full range of propeller sizes and locations. During a test, the correction factor was found by interpolation using the current propeller size and location.

$$\frac{V_{c_{fairing}}}{V_\infty} = k_{fairing} \tag{9}$$

To account for testing a propeller in a closed test section, the classic Glauert[23,24] correction was used. The flow around a propeller in a closed test section is different than the flow in free air. For a propeller producing thrust, the velocity in the propeller slipstream is greater than the nominal test section velocity. Since the same mass flux of air must pass ahead of the propeller as it does behind the propeller from continuity, the velocity outside of the slipstream must be lower. The pressure outside of the slipstream is also higher than the pressure ahead of the propeller, so the thrust measured is larger than the thrust produced at the same velocity in free air. Another way to describe the results is that the thrust measured would occur at a lower velocity in free air. To determine that lower velocity, the correction factor is found from

$$\frac{V_c}{V_\infty} = 1 - \frac{\tau\alpha}{2\sqrt{1+2\tau}} \tag{10}$$

where $\tau = T/\rho A V_\infty^2$ and $\alpha = A/C$. This correction is the first approximation of the iterative method described by Glauert, but for the propeller sizes, thrust values, and freestream speeds from this series of tests, the correction factor from Eq. 10 agrees with the full iterative method to a difference of less than 1%.

F. Verification of Performance Tests

Measuring accurate and repeatable performance data of the rotors from the balance is of great importance. The small forces from these rotors require sensitive equipment that increase the chance of experimental uncertainty overshadowing the results. In order to determine the Reynolds number effects on these small propellers, there must be a high level of confidence that the balance can repeatably measure small differences in thrust and torque that might be present at different Reynolds numbers.

A repeatability test is one measure of confidence in the balance data. Figures 3 and 4 show the results of three tests of the GWS 5×4.3 propeller. Two of the tests were done during the March 2013 wind tunnel

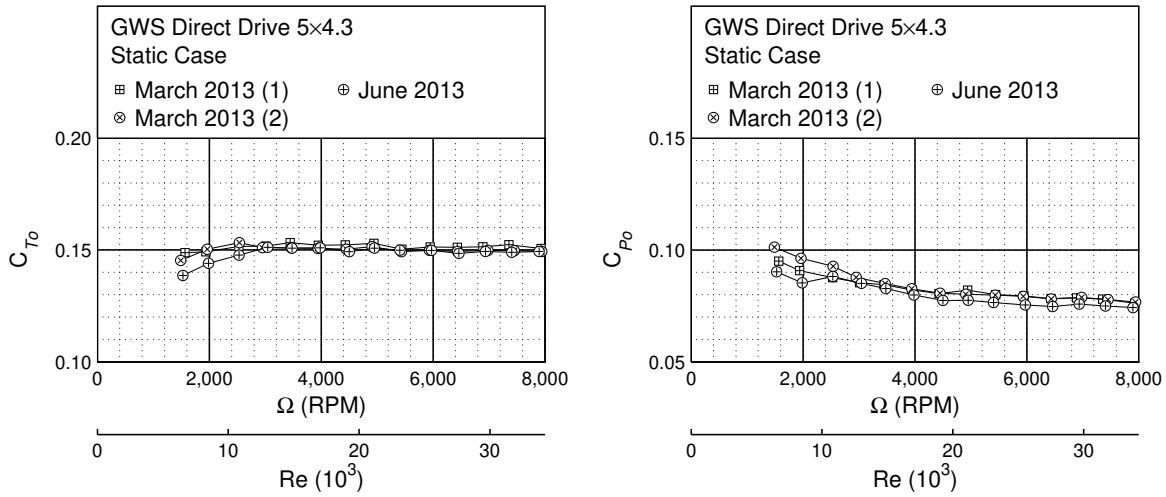

(a) (b)

Figure 3: Repeatability of the static performance of the GWS Direct Drive 5×4.3 propeller: (a) thrust coefficient and (b) power coefficient.

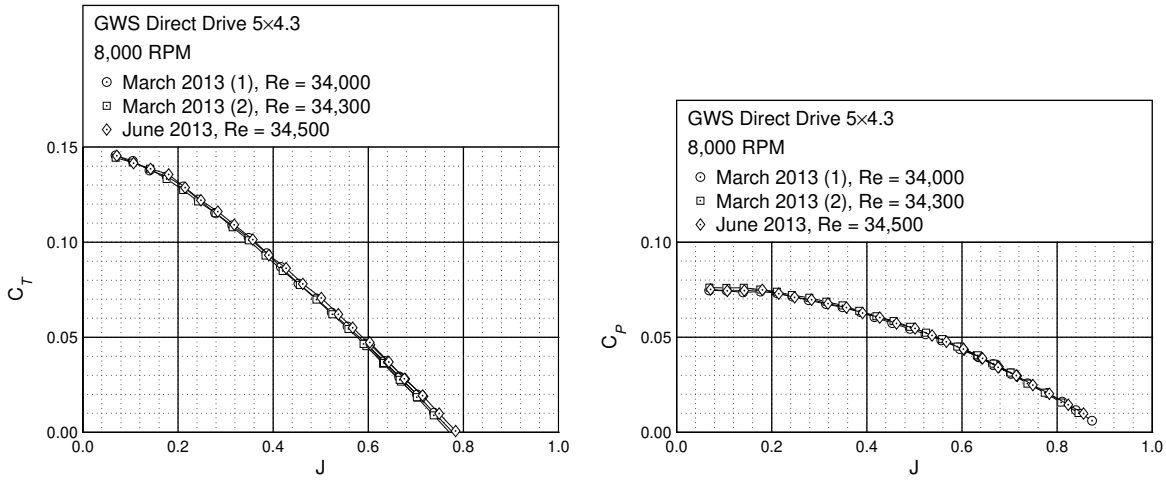

(a) (b)

Figure 4: Repeatability of the performance of the GWS Direct Drive 5×4.3 propeller at 8,000 RPM: (a) thrust coefficient and (b) power coefficient.

entry, and the third was done in the June 2013 wind tunnel entry. The first March test was performed near the beginning of the entry while the second test was performed near the end of the entry. As shown in the figures, the thrust and power during both the static and advancing-flow conditions agree for all three tests. Additional repeatability tests can be found in Deters.[19]

During the discussion on the experimental equipment, it was stated that the fairing was designed to remove the rig structure from the propeller slipstream and the freestream flow. To illustrate the need for the fairing, a comparison was done between propeller performance results taken with the current testing rig with results from the original testing rig designed by Brandt.[12] As shown in Fig. 5, the motor housing and the torque transducer were exposed to the propeller slipstream and freestream flow in the rig used by Brandt. These exposed parts created drag and lessened the measured thrust. Figure 6 shows the static performance results of the GWS Direct Drive 9×5 propeller from both testing rigs. The static thrust measured from the original rig is indeed less than the thrust measured from the current rig; the static power does not seem to

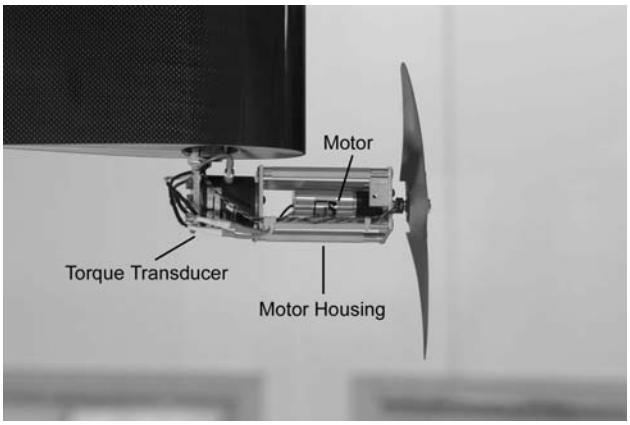

Figure 5: Original propeller testing rig designed by Brandt (figure taken from Brandt[12]).

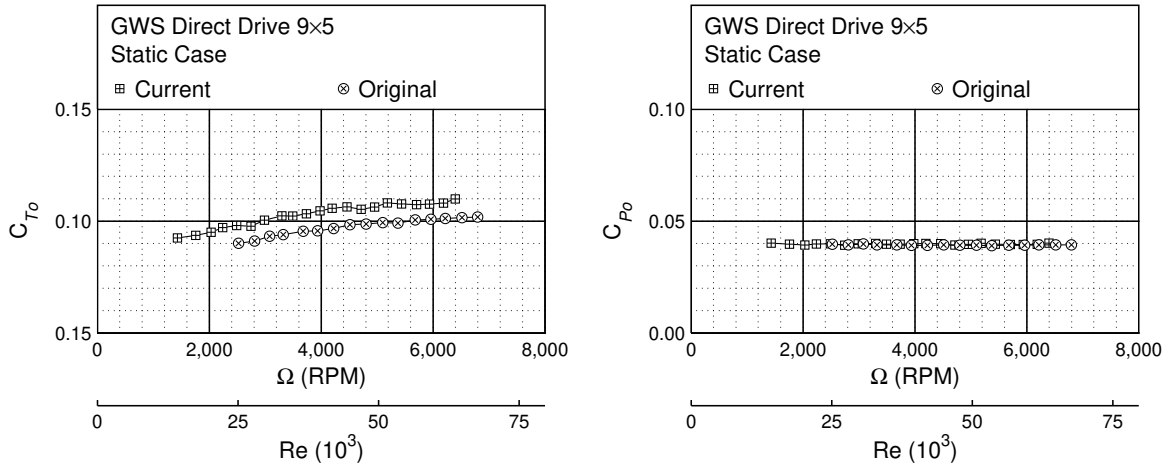

Figure 6: Static performance comparison of the GWS Direct Drive 9×5 propeller between the current rig and the original rig: (a) thrust coefficient and (b) power coefficient (original data taken from Brandt[12]).

be affected. The comparison between the two rigs for the same propeller running at 5,000 RPM are shown in Fig. 7. Thrust is again lower for the original rig, and the power is basically the same. The difference in measured thrust greatly changes the calculated maximum efficiency of the propeller, the advance ratio for the maximum efficiency, and the advance ratio for zero thrust.

Since many of the propellers tested were off-the-shelf, it was deemed interesting to determine how consistent the performance of one propeller was to another of the same type. Results from Merchant et al.[14] showed that two APC Thin Electric 16×12 propellers agreed well while two Zinger 16×6 varied in their measured thrust. For these tests, three GWS 2.5×0.8 and three GWS 5×4.3 propellers were statically tested and compared. From Fig. 8, the static performance of the GWS 2.5×0.8 propellers are consistent; however, a large difference is seen in the performance of the GWS 5×4.3 propellers (Fig. 9). The differences in the GWS 5×4.3 propellers are significant. To determine the reason for the similarity in the GWS 2.5×0.8 propellers and the large differences in the GWS 5×4.3 propellers, the geometry was measured for each propeller using PropellerScanner[25] (a more detailed discussion on PropellerScanner is included in Section III). From the measured geometry of the GWS 2.5×0.8 propellers (Fig. 10), the similarity for the static performance results is from the expected result that the three propellers have the same geometry. The measured geometry of the three GWS 5×4.3 propellers (Fig. 11) shows that, while the chord distribution is the same, the difference in the propellers is with the pitch. While the twist distribution for the three propeller is about the same, the

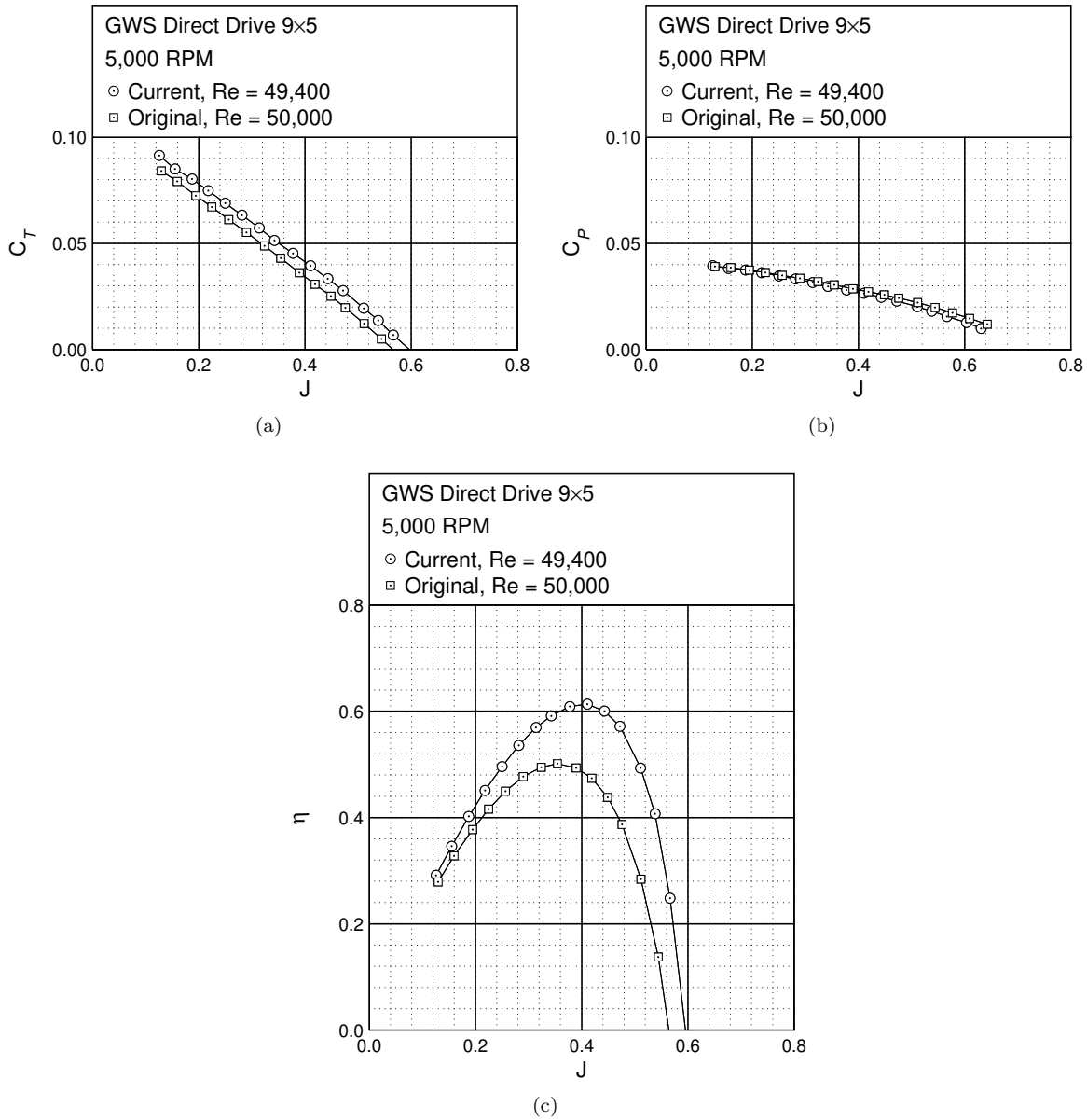

Figure 7: Performance comparison of the GWS Direct Drive 9×5 propeller between the current rig and the original rig at 5,000 RPM: (a) thrust coefficient, (b) power coefficient, and (c) efficiency curves (original data taken from Brandt[12]).

amount of pitch varies. From the geometry measurements, the differences in the performance is explained. Specimen 2 has a larger pitch, so it is expected that it would produce a larger thrust and power at a given rotation rate. Specimen 3 has a lower pitch, so it would produce a smaller thrust and power. This inconsistency between propellers shows that care should be taken when assuming the performance of one propeller based on the results of another.

Another way to measure the confidence of the balance data is to compare the results to another test. Smedresman et al.[20] from the University of Michigan have built a test stand to measure the performance of small propellers. A propeller tested at both the University of Michigan and UIUC is the Union U-80, and Fig. 12 shows a comparison between the different tests. As seen in the figure, the performance data agree. With the results from the repeatability tests and the results from the comparison to Michigan, performance data from the thrust and torque balance are reliable.

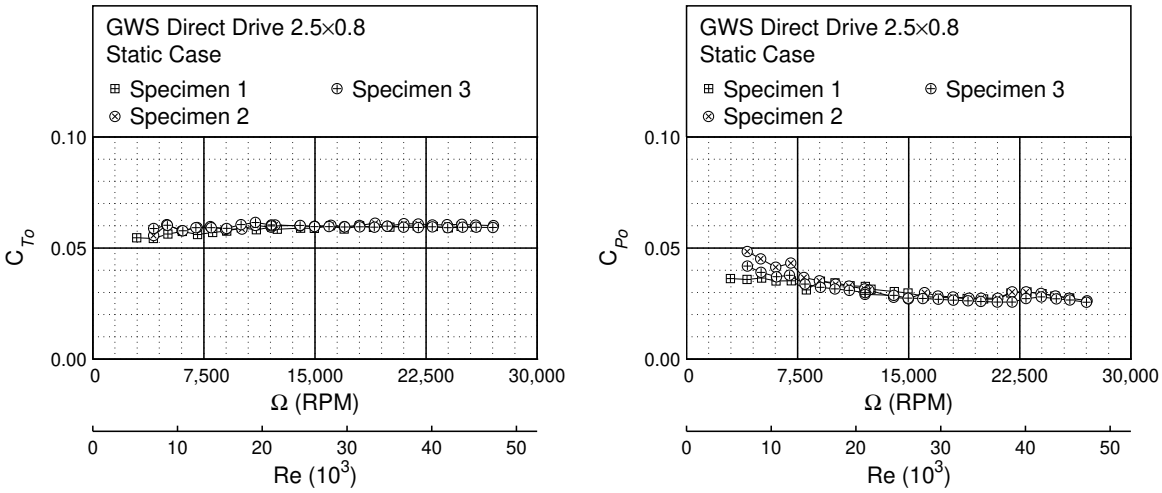

(a) (b)

Figure 8: Static performance of three GWS Direct Drive 2.5×0.8 propellers: (a) thrust coefficient and (b) power coefficient.

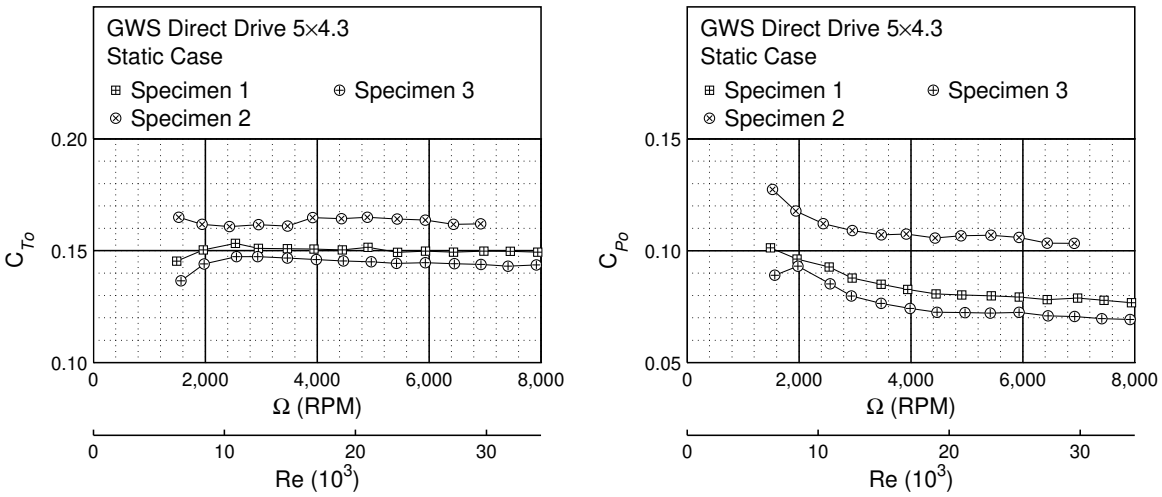

(a) (b)

Figure 9: Static performance of three GWS Direct Drive 5×4.3 propellers: (a) thrust coefficient and (b) power coefficient.

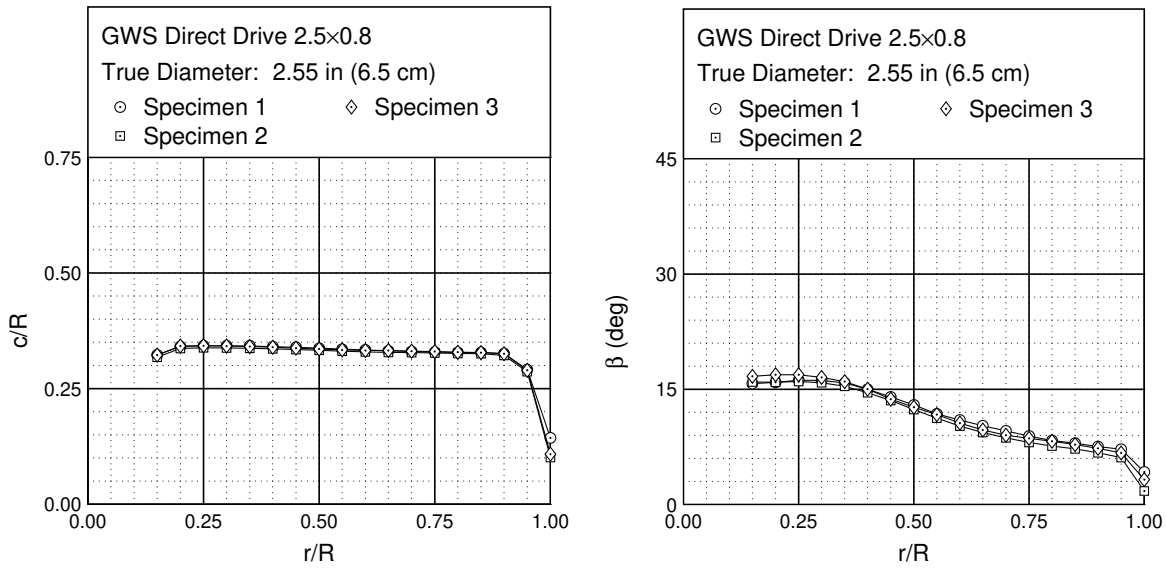

(a) (b)

Figure 10: Geometry comparison of the three GWS Direct Drive 2.5×0.8 propellers: (a) chord distribution and (b) twist distribution.

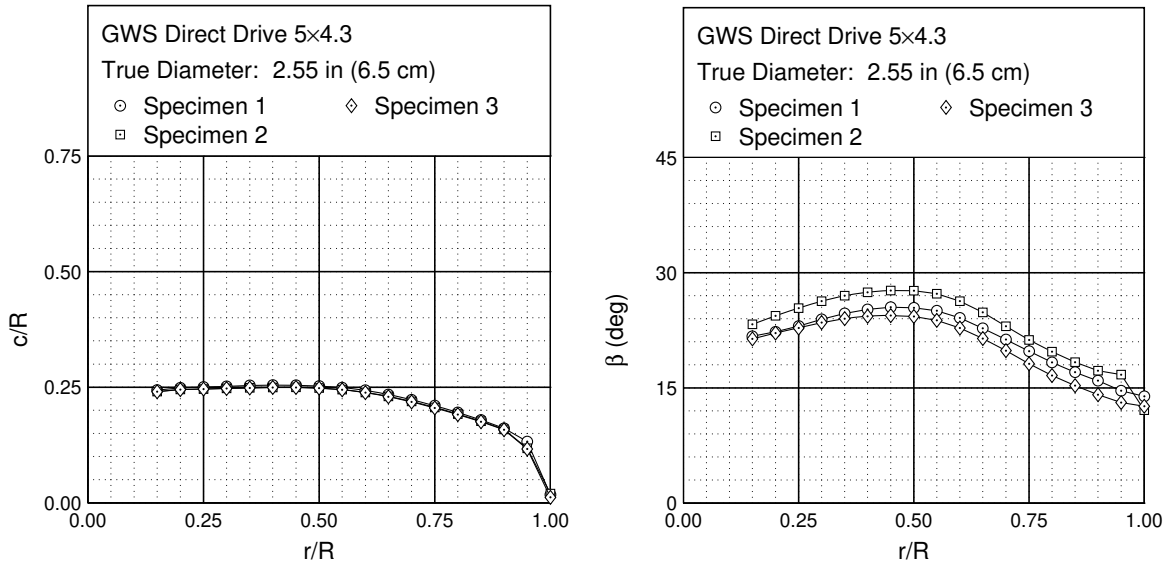

(a) (b)

Figure 11: Geometry comparison of the three GWS Direct Drive 5×4.3 propellers: (a) chord distribution and (b) twist distribution.

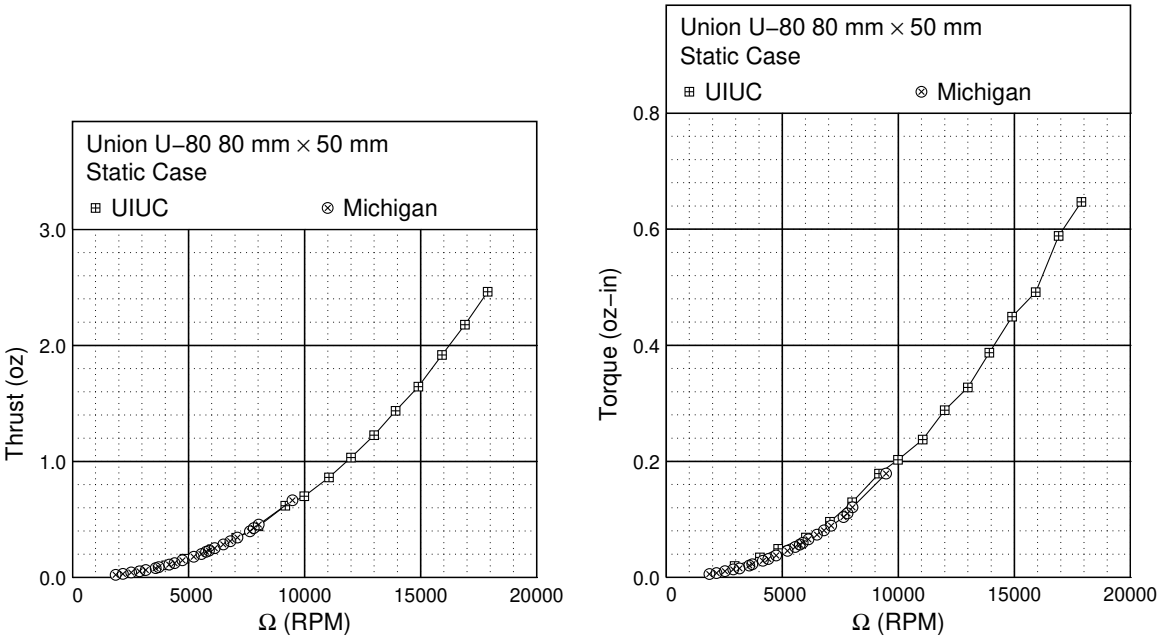

(a) (b)

Figure 12: Comparison between UIUC and Michigan static performance data of the Union U-80 propeller: (a) thrust and (b) torque (Michigan data taken from Smedresman et al.[20])

III. Propellers Tested

Two types of propellers were tested in this research: off-the-shelf propellers and in-house 3D-printed propellers. The off-the-shelf propellers are widely available and come in a variety of sizes. Nevertheless, it is difficult to find propellers that are scaled, i.e. have different diameters but have the same twist distribution and the same chord-to-radius distribution. For this reason, 3D-printed propellers with diameters of 5 and 9 in were designed, built, and tested. With these 3D-printed propellers, the geometry could be specified.

A range of diameters were tested for the off-the-shelf propellers. The largest diameter tested was 9 in and the smallest was 2.25 in. In total, the performance of 27 off-the-shelf propellers was measured, and a list of these propellers with their true diameters is given in Table 1. The chord and twist distributions for each propeller were measured using the PropellerScanner software created by Hepperle.[25] The program uses images of the side and top view of the propeller to calculate the chord and twist distribution. PropellerScanner is designed to measure the chord and twist of a 2-blade propeller; geometry results shown in this report are the average of both blades. While this method might not be as accurate as physically measuring slices of the propeller, PropellerScanner provides a quick method to compare the geometry of many propellers without the need to slice and destroy the propeller. Uhlig et al.[13,26] compared the chord and twist distributions of a propeller measured using PropellerScanner and from slices of the propeller. It was shown that the chord distribution agreed well, but the twist distribution from PropellerScanner underestimated the physically measured twist. The finite thickness of the propeller airfoil accounts for the differences between the results from PropellerScanner and the true propeller chord and twist distributions. Results from the PropellerScanner measurements are available in Deters et al.[18,19] and on the UIUC propeller database.[27]

From the PropellerScanner results, it is clear that manufacturers use a large variety of chord and twist distributions in their propellers. Even propellers from the same manufacturer that have the same pitch-to-diameter ratio generally will not have the same chord or twist distributions. The geometry of the GWS propellers shows this variety well. The GWS propellers tested were divided into two categories based on their planform shape, and an example of each planform is given in Fig. 13. For the rectangular planform propellers (Fig. 14), the shape of the chord distribution is basically the same for all four propellers with only the magnitude of the chord-to-radius values changing; smaller diameter propellers have larger c/R.

Table 1: Summary of off-the-shelf propellers tested

Manufacturer	Type	Propeller	Diameter (in)
APC	Free Flight	4.2×4	4.20
		9×4	9.00
	Sport	4.2×2	4.20
		9×6	9.00
E-Flite	–	100 mm×70 mm	5.10
GWS	Direct Drive	2.5×0.8	2.55
		2.5×1	2.55
		3×2	3.25
		3×3	3.20
		4×2.5	4.00
		4×4	4.00
		4.5×3	4.50
		4.5×4	4.50
		5×3	5.00
		5×4.3	5.00
		9×5	9.00
KP	Folding	96 mm×70 mm	3.80
Micro Invent	2-Blade	3.2×2.2	3.20
		4×2.7	3.95
		5×3.5	4.90
	3-Blade	4.3×3.5	4.40
		5×4	4.90
Plantraco	–	57 mm×20 mm	2.25
		Tri-Turbofan	2.55
		100 mm×80 mm	4.00
Union	U-80	80 mm×50 mm	3.15
Vapor	–	140 mm×45 mm	5.50

(a) GWS 3×2 with a rectangular planform.

(b) GWS 3×3 with a tapered planform.

Figure 13: Example planforms of the GWS propellers.

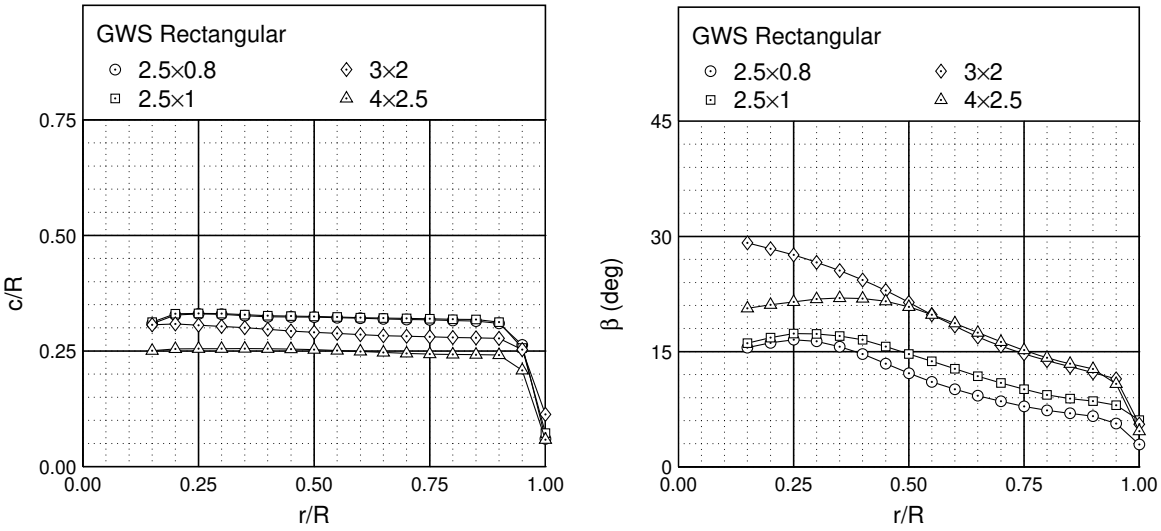

(a) (b)

Figure 14: Geometry comparison of the GWS propellers with a rectangular planform: (a) chord distribution and (b) twist distribution.

However, the shape of the twist distribution is not the same for all of the propellers. Even though the 3×2 and 4×2.5 propellers have about the same pitch, the twist distribution is clearly not the same for the for the inboard portion of the propellers. The differences seen with the tapered propellers are even more pronounced (Fig. 15). While the shape of the twist distribution is very similar between the two 5-in propellers, it does not match with the other diameters. The 3×3 and 4×4 propellers have about the same pitch and twist distribution, but the c/R is greater for the 3-in propeller. Of all of the off-the-shelf propellers tested, the APC propellers were the closest in matching chord and twist distributions between propellers of different diameters. Figure 16 shows the geometry of the 4.2×2 and 9×4 propellers, which have about the same pitch-to-diameter ratio. The twist distribution of the two propellers is basically the same, and the shape of the chord distribution is the same except that the 4.2-in propeller has a larger c/R.

With the large variety in chord and twist distributions found in the off-the-shelf propellers, it is difficult to make comparisons between the propellers. While determining the general Reynolds number effects on these propellers could still be made, comparisons between propellers of different diameters but having the same chord and twist distributions could not be done. For this reason, 3D-printed propellers with diameters of 5 and 9 in were designed, built, and tested. With these 3D-printed propellers, the geometry could be specified. An overview on the design of the 3D-printed propellers follows with a more detailed discussion available in Deters.[19]

Each propeller was built using the MechSE Rapid Prototyping Lab at the University of Illinois at Urbana-Champaign. To reduce the number of parts to manufacture, the propeller blades and hub were built as

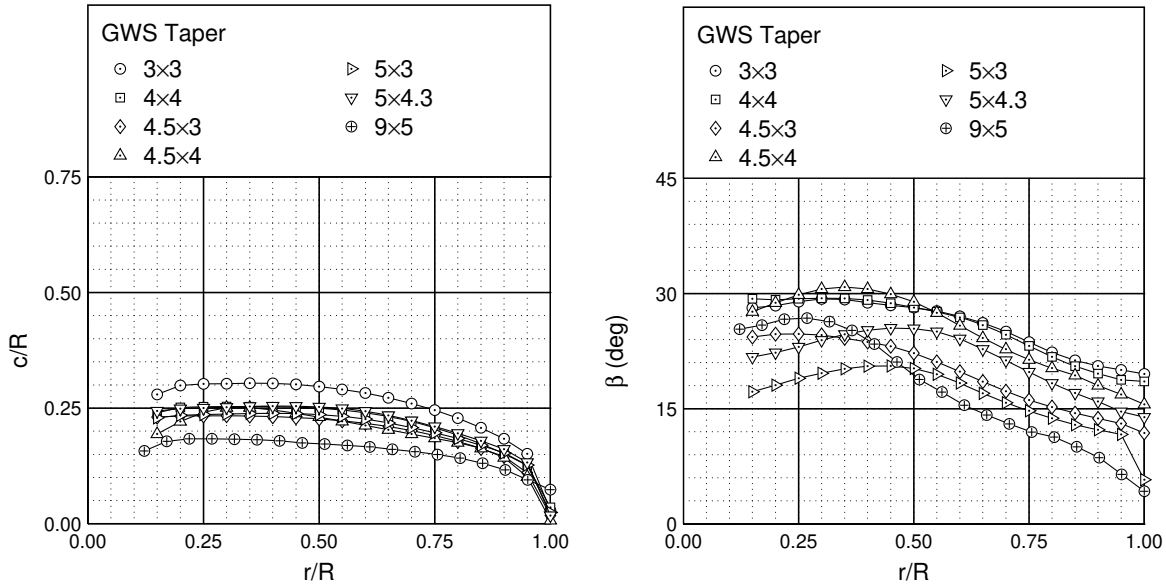

(a) (b)

Figure 15: Geometry comparison of the GWS propellers with a tapered planform: (a) chord distribution and (b) twist distribution.

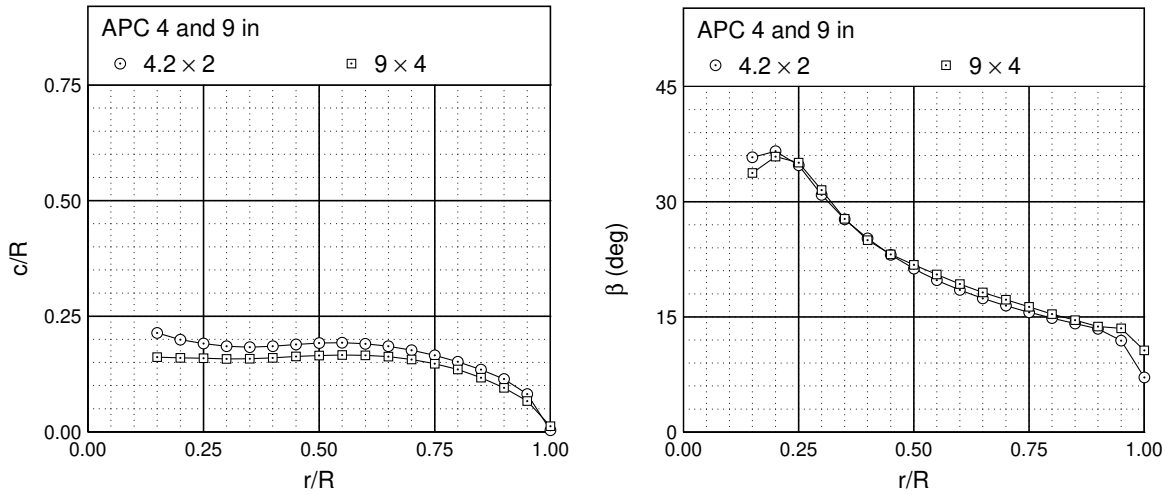

(a) (b)

Figure 16: Geometry comparison of the 4.2 and 9-in APC propellers with a similar pitch-to-diameter ratio: (a) chord distribution and (b) twist distribution.

separate parts (Fig. 17). The propeller blades were manufactured using an Objet Eden 350 16-micron layer 3D printer with VeroBlack used as the material. The hubs were built using a Viper stereolithography apparatus (SLA). The blades were then attached to the hub and secured in place with screws. This separate part method allowed the pitch of the propeller to be changed by only requiring a new hub to be built. Four types of hubs were manufactured for the 2-bladed propellers based on the desired pitch of the propeller. Figure 18 shows the four hubs designed to change the pitch. The first hub is designed to test the propeller at its original pitch angle, the second decreases the pitch by 10 deg, the third decreases the pitch by 5 deg,

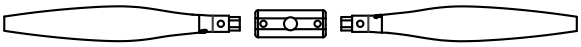

Figure 17: Front view of the separated blades and hub of a 2-bladed NR640 propeller. The small outer holes on the hub and the holes on the blade align, and each blade is attached to the hub with a screw and nut.

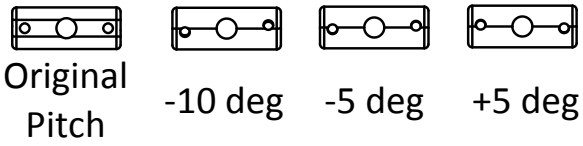

Figure 18: Hub designs for changing the pitch of the propellers.

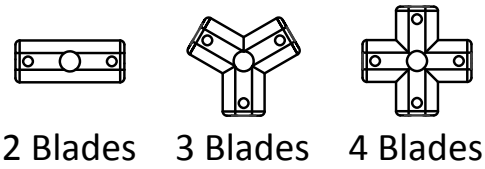

Figure 19: Hub designs for 2-, 3-, and 4-blade propellers.

and the fourth hub increases the pitch by 5 deg. Propellers with three and four blades could also be tested and only required additional blades and a new hub (Fig. 19).

The first propeller designed was based on the 10-ft diameter Navy propeller 5868-9 described in NACA Report 640.[28] The 5868-9 propeller used a Clark Y airfoil with different thickness ratios for the blade sections and was tested in 2-, 3-, and 4-blade configurations at different pitch angles. For this research, the scaled 5868-9 propeller with a pitch of 15 deg was designated NR640. The chord and twist distributions of the NR640 matches the Navy 5868-9 and are shown in Fig. 20. Like the full-scaled version, the airfoil used for the NR640 is based on the Clark Y with the thickness changing along the span. The thickness ratio distribution for the NR640 is also shown in Fig. 20. To aid in manufacturing, the trailing edge of the Clark Y was thickened using XFOIL.[29] Figure 21 shows the modified Clark Y airfoils with the largest and smallest thickness-to-chord ratio. To change the thickness ratio of the airfoil, XFOIL was used.

The second propeller was designed to minimize the induced losses of the propeller. A 9-in propeller with a pitch of 6.75 in (17.7 deg) was chosen for the design. The 6.75-in pitch provides a pitch-to-diameter ratio of 0.75 and falls within the common range of pitch-to-diameter ratios for off-the-shelf propellers. Design of the new propeller was done using the PROPID inverse design code.[27,30] A baseline propeller with a rectangular blade having a c/R of 0.18 was used as a starting point. The SD7003 airfoil[3] was used for the baseline propeller. This airfoil is 8.5% thick and has good performance at low Reynolds numbers. The design point for the new propeller was at 5,000 RPM with an advance ratio of 0.65, which was the advance ratio for maximum efficiency of the baseline propeller. PROPID iterated on the chord and twist of the propeller so all of the propeller blade stations matched the lift coefficient and axial induction factor at the 75% blade station.

To make sure that the propellers built with the 3D printer did not have requirements that were smaller than the resolution of the printer, the trailing edge of the new propeller was designed to be a constant 0.003 in for the 5-in diameter propellers. This constraint required new airfoils to be designed with the desired trailing edge thickness. Three new airfoils with a maximum thickness of 8.5% were designed based on the desired trailing edge thickness at the 45% blade station, the 75% blade station, and at the tip. Each airfoil was designed using PROFOIL, an airfoil inverse design program developed by Selig.[31,32] However, the propellers built with the new airfoils were less than satisfactory. The propeller blades were very flexible and would deform easily. To strengthen the propeller blades, new airfoils were designed using PROFOIL. The desired trailing edge thickness for a 5-in propeller was increased to 0.005 in, and the maximum thickness of each airfoil was increased to 12%. The resulting propellers were much stronger and held their shape much better.

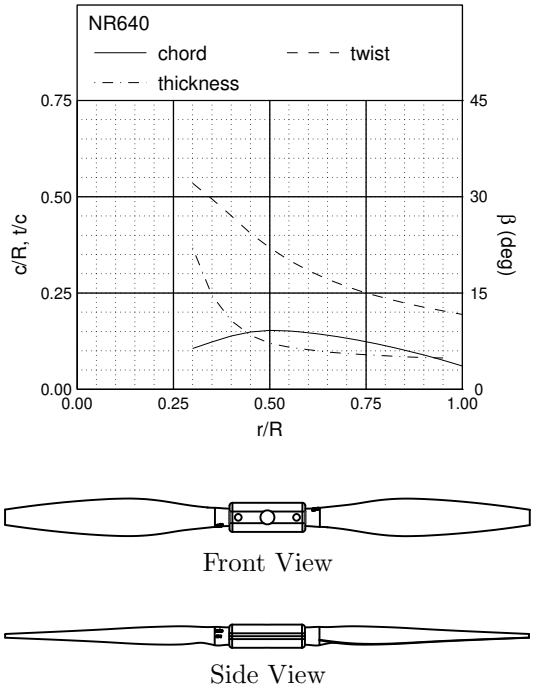

Figure 20: NR640 geometric characteristics.

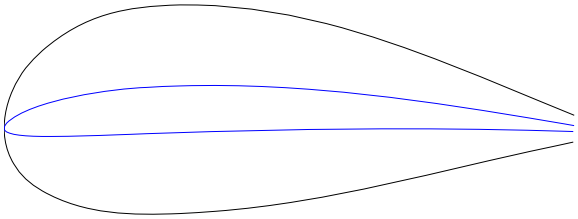

Figure 21: Modified Clark Y airfoils near the hub and tip of the NR640 propeller.

The new propeller was named DA4052, and the geometry is provided in Fig. 22. Figures 23, 24, and 25 show the shape of the three 12% thick airfoils designed using PROFOIL. The coordinates of the three airfoils are provided in Appendix A.

The last two propellers were simple rectangular blades with a constant pitch of 6.75 in for the 9-in propellers and 3.75 in for the 5-in propellers. One propeller was designed with a c/R of 0.18 and was named DA4002. The other had a c/R of 0.23 and was named DA4022. Both propellers used the SDA1075 airfoil for the full blade. The geometry of the DA4002 is given in Fig. 26, and the geometry of the DA4022 is the same as the DA4002 with only the c/R at 0.23.

A summary of the 3D-printed propellers tested is given in Table 2. With the different hubs available, all of the 3D-printed propellers were tested with more than two blades or at different pitch angles. As stated earlier, the DA4052, DA4002, and DA4022 were designed with a p/D of 0.75 where that corresponds to 6.75 in for the 9-in propellers and 3.75 in for the 5-in propellers. In terms of an angle, the pitch is 17.7 deg. The table provides the pitch for the propellers in inches and in degrees for clarity.

In order to judge the manufacturing accuracy of the 3D-printed propellers, the geometries of the NR640 and DA4002 propellers were measured using PropScanner. Both the 5-in and 9-in versions were compared to the designed geometry, and the results are shown in Fig. 27. While the chord distributions of the 3D-printed propellers match the designed chord distribution, there is some difference in the twist distribution. For the last 35% of the blade, the two manufactured propellers are similar to each other except around 90% where

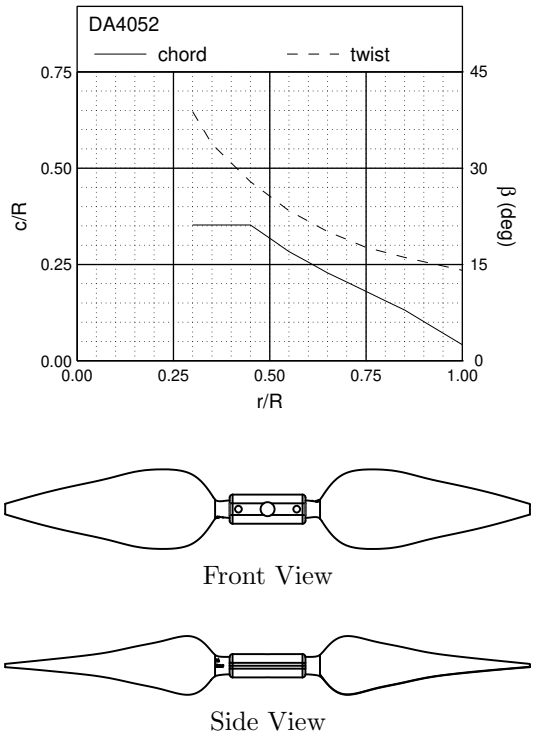

Figure 22: DA4052 geometric characteristics.

Figure 23: Propeller airfoil for the 45% blade station (SDA1045).

the 9-in propeller has a smaller twist angle. Both manufactured propellers have twist angles about 1 to 2 deg larger than the designed twist for the outer 35%. For the inner portion of the blade, the two manufactured propellers do not agree in twist. The 9-in propeller has a slightly larger twist angle than the 5-in. From about 40% to 60%, the twist of the 5-in propeller matches the designed twist. With this geometry difference between the 5- and 9-in propellers, it is expected that there will be differences in their performance.

The geometry comparison of the DA4002 is shown in Fig. 27. Similar to the NR640, the chord distribution of the manufactured DA4002 propellers match the designed. The twist distributions for the 5- and 9-in manufactured propellers are in close agreement and are about 1 to 2 deg larger than the designed twist. As mentioned earlier, Uhlig et al.[13,26] showed that PropScanner underestimated the twist angle for one of the propellers they measured, so the twist values measured for the NR640 and DA4002 could be further off. However, since the twist from the 5- and 9-in versions of both propellers were measured to be very close to the designed case, it is likely that the manufacturing process was fairly accurate. The most likely cause between the difference in accuracy seen in the NR640 and DA4002 propellers is airfoil thickness. The DA4002 propeller has a larger chord than the NR640 along the entire span. This larger chord led to a stiffer blade especially near the tips.

Figure 24: Propeller airfoil for the 75% blade station (SDA1075).

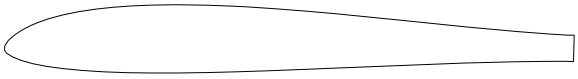

Figure 25: Propeller airfoil for the tip (SDA1100).

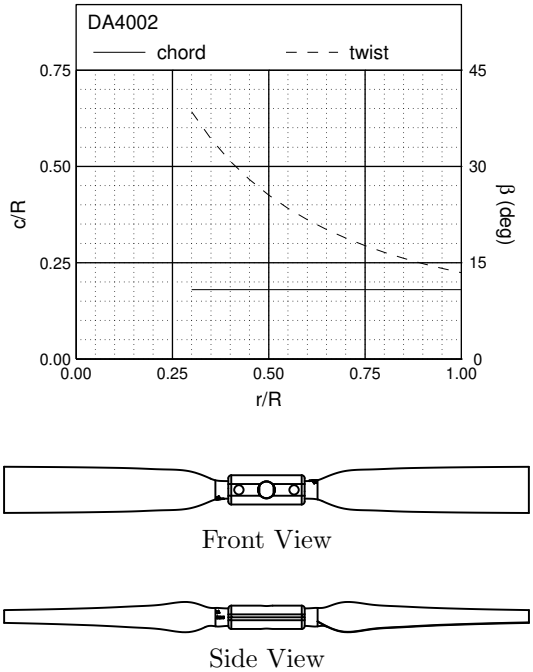

Figure 26: DA4002 geometric characteristics.

Table 2: Summary of 3D-printed propellers tested

Propeller	Diameter (in)	Pitch (in)	Pitch (deg)	p/D	Number of Blades
NR640	5	3.16	15	0.63	2
					3
					4
		4.29	20	0.86	2
	9	5.68	15	0.63	2
					3
					4
		7.72	20	0.68	2
DA4052	5	3.75	17.7	0.75	2
					3
					4
		1.58	7.7	0.32	2
		2.65	12.7	0.53	
		4.92	22.7	0.98	
	9	6.75	17.7	0.75	2
					3
		2.85	7.7	0.32	2
		4.76	12.7	0.53	
		8.85	22.7	0.98	
DA4002	5	1.58	7.7	0.32	2
		2.65	12.7	0.53	
		3.75	17.7	0.75	
		4.92	22.7	0.98	
	9	2.85	7.7	0.32	2
		4.76	12.7	0.53	
		6.75	17.7	0.75	
		8.95	22.7	0.98	
DA4022	5	3.75	17.7	0.75	2
					3
					4
	9	6.75	17.7	0.75	2
					3
					4

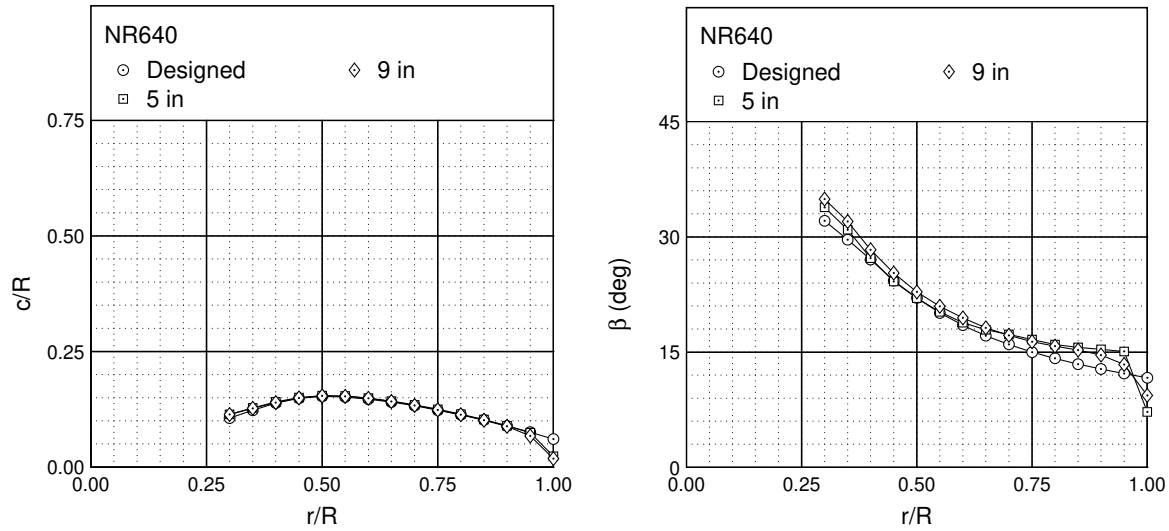

(a) (b)

Figure 27: NR640 geometry comparison of the designed, 5-in, and 9-in propellers: (a) chord distribution and (b) twist distribution.

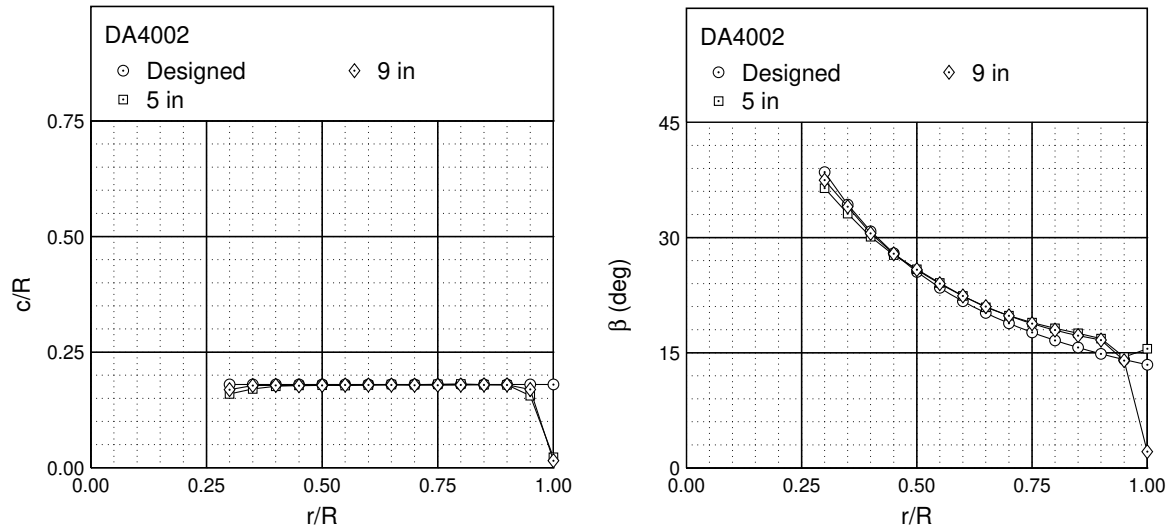

(a) (b)

Figure 28: DA4002 geometry comparison of the designed, 5-in, and 9-in propellers: (a) chord distribution and (b) twist distribution.

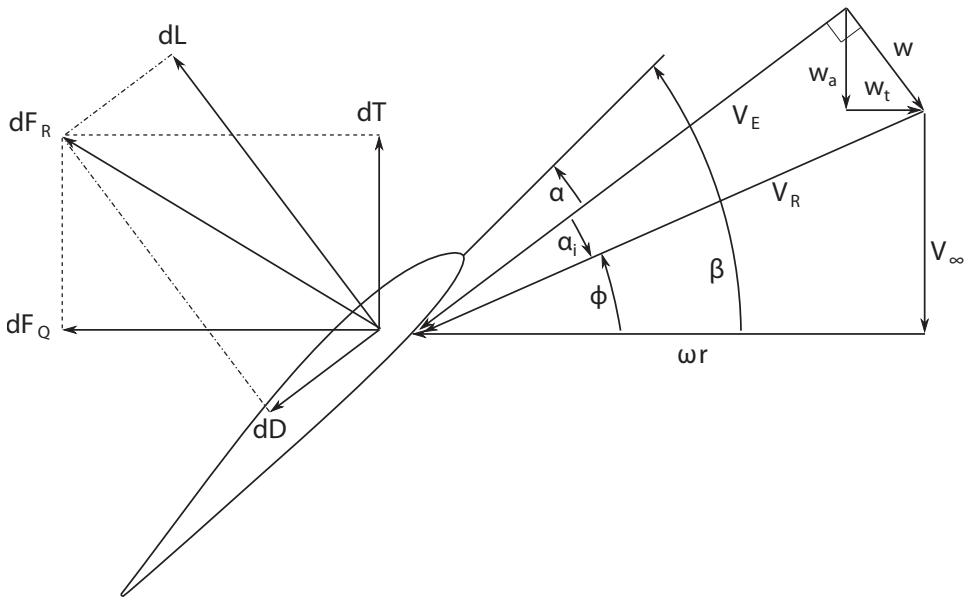

Figure 29: Blade element of a propeller with the corresponding forces and velocities (adapted from McCormick[35]).

IV. Expected Propeller Results from Theory

Before the results from the performance and slipstream tests are presented and discussed, this section reviews the expected results from propeller theory, specifically the determination of propeller forces from blade element theory. Results from theory are discussed, but the theory is not derived. Derivations of these theories are presented in many sources such as Johnson,[33] Leishman,[34] and McCormick.[35] The naming scheme for the variables in the discussion is similar to that used by McCormick.[35]

The forces acting on a single blade element of a propeller at a radius r from the propeller center are shown in Fig. 29 (adapted from McCormick[35]). The incremental thrust and torque can be put in terms of the lift and drag by

$$dT = dL\cos(\phi + \alpha_i) - dD\sin(\phi + \alpha_i) \tag{11}$$

$$dQ = r\left[dL\sin(\phi + \alpha_i) + dD\cos(\phi + \alpha_i)\right] \tag{12}$$

In terms of the lift and drag coefficients, the incremental forces can be integrated to find the propeller thrust and power coefficients as shown in Eqs. 13 and 14.

$$C_T = \frac{\pi}{8}\int_{x_h}^{1}\left(J^2 + \pi^2 x^2\right)\sigma_1\cos^2\alpha_i\left[C_l\cos(\phi + \alpha_i) - C_d\sin(\phi + \alpha_i)\right]dx \tag{13}$$

$$C_P = \frac{\pi}{8}\int_{x_h}^{1}\pi x\left(J^2 + \pi^2 x^2\right)\sigma_1\cos^2\alpha_i\left[C_l\sin(\phi + \alpha_i) + C_d\cos(\phi + \alpha_i)\right]dx \tag{14}$$

The variables x and σ_1 are defined by Eqs. 15 and 16, respectively, x_h is the hub location where the propeller blade starts, B is the number of blades, R is propeller radius, and c is the chord length.

$$x = \frac{r}{R} \tag{15}$$

$$\sigma_1 = \frac{Bc}{\pi R} \tag{16}$$

From the thrust and power coefficient equations (Eqs. 13 and 14), the effect of Reynolds number can be discussed. Airfoil tests at Reynolds numbers below 500,000 have shown that the lift coefficient decreases and

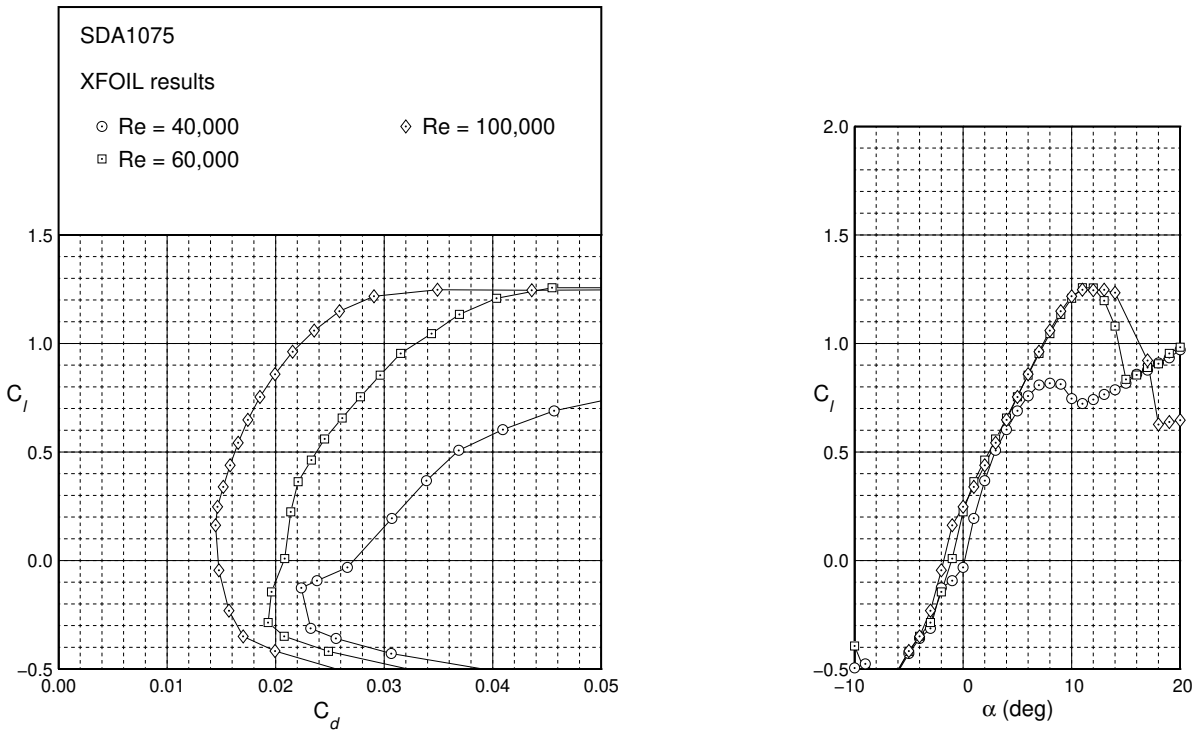

Figure 30: Drag polar for the SDA1075 airfoil from XFOIL analysis.

the drag coefficient increases as the Reynolds number decreases. The effects on the lift and drag coefficients are more pronounced at Reynolds numbers below 100,000.[1–7] If the lift coefficient decreases, both the thrust and power coefficients will decrease, but typically the decrease in thrust will be more due to the cosine term. If the drag coefficient increases, the thrust coefficient will decrease and the power coefficient will increase. Ideally a designer wants a propeller that will produce a given thrust at the lowest power. A decrease in thrust and an increase in power with decreasing Reynolds number cause a propeller to be less efficient.

To illustrate the effect of Reynolds number on the performance of a propeller, the 9-in DA4002 propeller with two blades was analyzed in PROPID, a BEMT code developed by Prof. Selig.[27,30] As discussed in Section III, the blades of the DA4002 are rectangular and have a c/R ratio of 0.18. The SDA1075 airfoil is used all along the blade except near the hub, and the airfoil aerodynamic characteristics are shown in Fig. 30. These aerodynamic characteristics were found using XFOIL and show that, as the Reynolds number decreases, the lift coefficient decreases and the drag coefficient increases. The change in the lift and drag with Reynolds number can be explained by the behavior of the boundary layer. At these Reynolds numbers a laminar separation bubble can form on the airfoil.[1,36] Figure 31 from McGranahan[36] shows a schematic of a laminar separation bubble. Point 'S' is where the laminar flow separates from the airfoil due to an adverse pressure gradient. The flow off of the airfoil surface eventually transitions to turbulent and is shown in the figure as point 'T.' If the more energetic flow reattaches to the airfoil, it is at point 'R' in the figure. After reattachment, the flow continues downstream as a turbulent boundary layer. The size of the laminar separation bubble will affect the lift and drag of the airfoil. A larger bubble will decrease the lift and increase the drag more, and the bubble typically grows as the Reynolds number decreases.

The DA4002 propeller was analyzed at rotational rates of 2,000, 3,000, 4,000, and 5,000 RPM, which correspond to Reynolds numbers based on the rotational velocity and chord at the 75% station of 25,300, 37,900, 50,600, and 63,200. Figure 32 shows how the Reynolds number along the propeller blade changes with different rotational rates. This figure shows the Reynolds number calculated from PROPID at an advance ratio of 0.60. As the rotational rate increases, the variation in Reynolds number along the span increases, and a larger portion of the blade sees the benefits of larger Reynolds numbers.

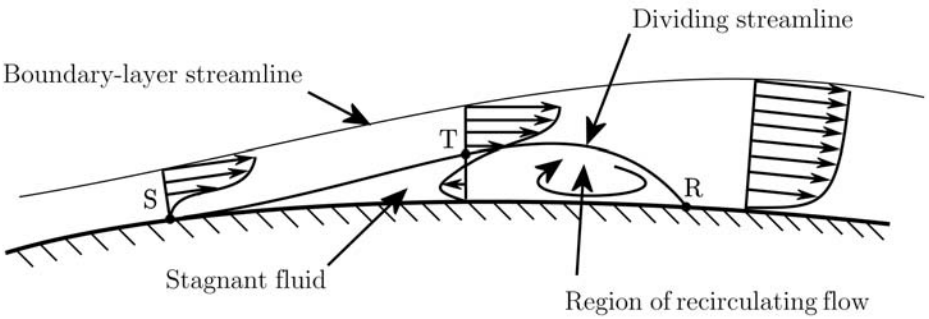

Figure 31: Laminar separation bubble schematic from McGranahan.[36]

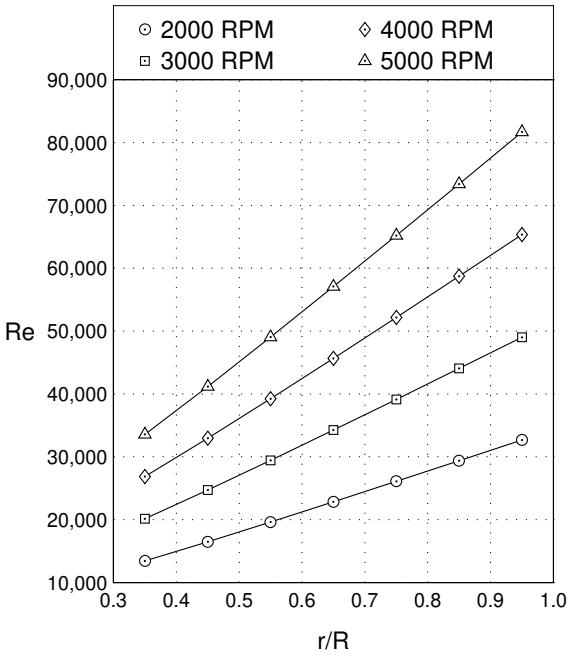

Figure 32: Reynolds number variation along the propeller blade for the DA4002 9×6.75 at an advance ratio of 0.60.

As shown in Fig. 33, the thrust coefficient increases as the rotational rate, and therefore the Reynolds number, increases. This thrust coefficient increase is seen for all the advance ratios. The Reynolds number effect on the power coefficient (Fig. 34) is different in that the power coefficient decreases with increasing Reynolds number at lower advance ratios but then increases with increasing Reynolds number at larger advance ratios. To help explain the Reynolds number effects on C_T and C_P, the lift and drag coefficients along the propeller blade are plotted in Figs. 35a and 35b, respectively, for two rotational rates and two advance ratios. For both advance ratios, the increase in Reynolds number (rotation rate) leads to an increase in the lift coefficient and a decrease in the drag coefficient. Both of these changes are beneficial to increasing the thrust coefficient as shown in Eq. 13. For the power coefficient, a decrease in the drag coefficient is beneficial while an increase in lift is not (Eq. 14). At J=0.30, the drag coefficient decrease is larger than at J=0.60, and the lift coefficient increase is smaller at J=0.30 than at J=0.60. These differences at the two advance ratios explain the reason why a larger Reynolds number is beneficial to the power coefficient at lower advance ratios but not at the higher advance ratios. The larger decrease in the drag coefficient at

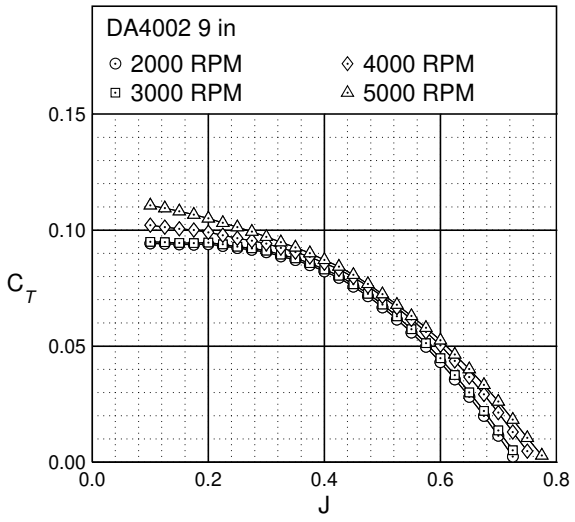

Figure 33: DA4002 9×6.75 thrust coefficient from PROPID.

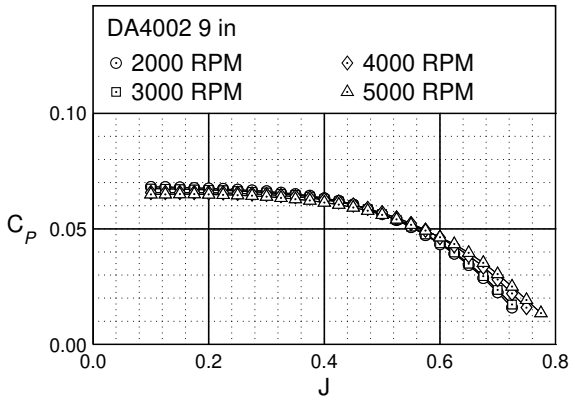

Figure 34: DA4002 9×6.75 power coefficient from PROPID.

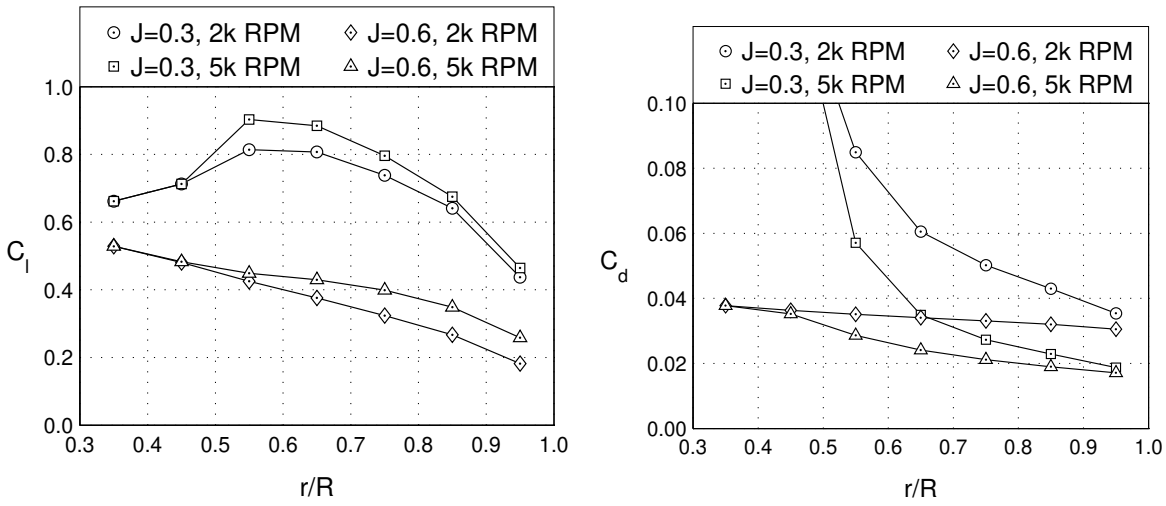

(a) (b)

Figure 35: Lift coefficient (a) and drag coefficient (b) distributions for the DA4002 9×6.75 at two rotational rates and two advance ratios.

the lower advance ratios is enough to offset the lift coefficient increase, but at the higher advance ratios, the drag decrease is less and the larger increase in the lift coefficient dominates.

Nevertheless, for all of the advance ratios, the differences in the power coefficient are not as large as differences in the thrust coefficient, and the increase in the thrust coefficient is the reason for the increase in the efficiency shown in Fig. 36. At lower advance ratios, the differences in the efficiency are not as large as those near the point of maximum efficiency. Beyond the advance ratio for maximum efficiency, the curves spread out and the higher Reynolds number cases will cross the line of zero efficiency at a larger advance ratio. This delay in zero efficiency is due to the propeller being able to produce more thrust (C_T) at larger advance ratios as was shown in Fig. 33. The efficiency plot also shows that the maximum efficiency achieved for this propeller at these Reynolds numbers is around 70%. According to McCormick,[35] a well-design propeller typically has an efficiency around 85%. The difference of 15% in maximum efficiency highlights the large performance loss that occurs when operating propellers at Reynolds numbers around 100,000 and less.

Another expected result from blade element theory deals with scaling propellers. From the equations for the thrust and power coefficients (Eqs. 13 and 14), the size of the propeller should not matter since all of the

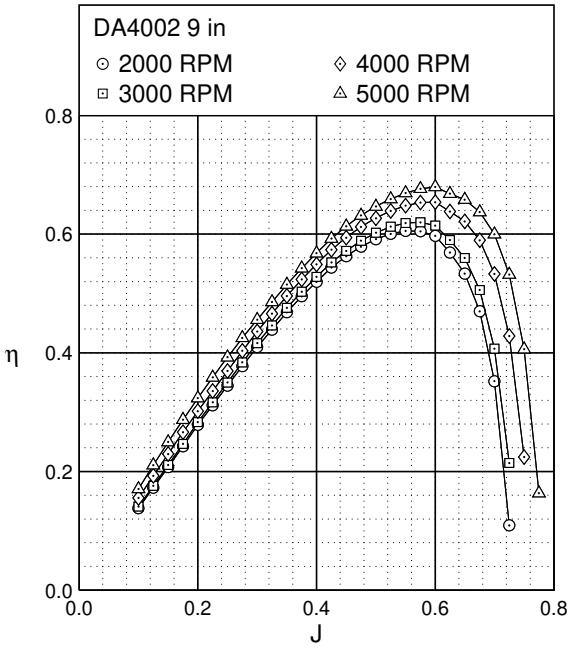

Figure 36: DA4002 9×6.75 efficiency curves from PROPID.

terms are nondimensional. However, the effect of the propeller size is important to these equations in that it affects the Reynolds number and the Mach number, which in turn will affect C_l, C_d, and α_i. The propellers studied in this research are small enough that the Mach number will not be a factor, but as shown earlier, the Reynolds number will have an effect. If two propellers of different sizes are tested at the same Reynolds number, then the C_T and C_P values for both propellers should be the same when the advance ratio is the same. To have propellers of different sizes have the same Reynolds number requires the smaller propeller to spin at a higher rotational rate. PROPID was used to simulate a 5-in and 9-in DA4002 propeller. The 9-in propeller had a rotational rate of 2,000 RPM, and the 5-in had a rotational rate of 6,480 RPM. These rates correspond to a Reynolds number of 25,300. The results for C_T, C_P, and η are shown in Fig. 37 and are exactly the same for both propellers. While the coefficients are the same, some of the dimensional values will be different. The thrust for both propellers is the same, but the disk loading for the 5-in propeller will be 3.24 times the 9-in propeller. Also the power for the 5-in propeller will be 1.8 times the power of the 9-in propeller. The thrust and power values show that to produce the same thrust, the smaller 5-in propeller will require more power.

V. Performance Testing Results

Static and advancing-flow performance tests were done on all of the propellers listed in Tables 1 and 2. Results for some of the propellers will be discussed in this section to demonstrate the Reynolds number effects. Performance results for all of the propellers can be found in Deters et al.[18,19] and on the UIUC propeller database.[27]

A. Static Tests

Figure 38 shows the results of the static tests on the four APC propellers. The thrust and power coefficients are plotted against the Reynolds number in order to compare the four propellers. The magnitude of each performance curves follows the pitch-to-diameter ratio of the propeller. The 4.2×4 propeller has the highest ratio, so its thrust and power curves have the largest values. Since the 4.2×2 and 9×4 have about the same ratio and, as shown in Fig. 16, about the same twist and chord distributions, it is not surprising that results for the two propellers are nearly the same at the same Reynolds number. The 4.2×2 propeller has larger

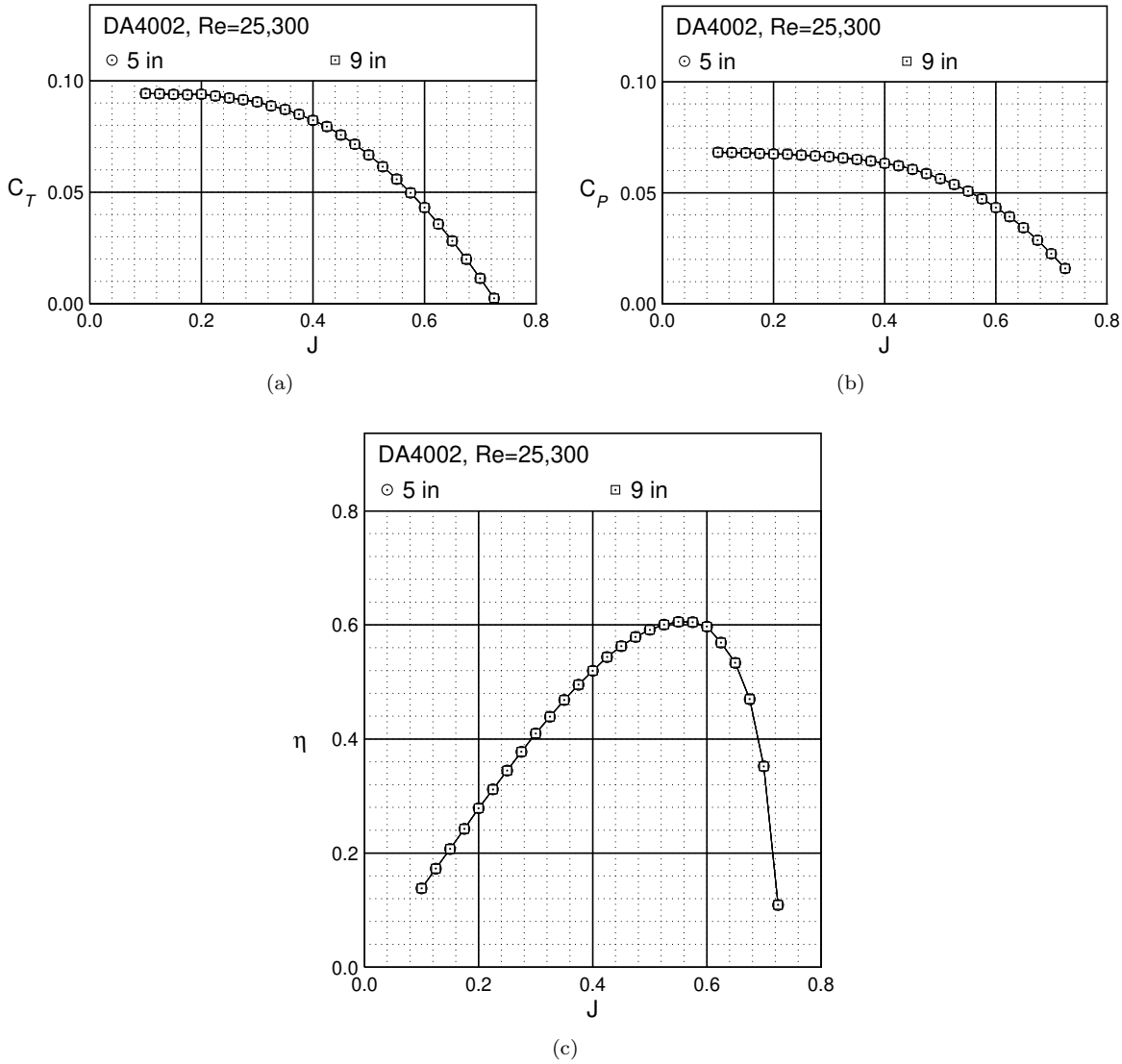

Figure 37: Performance comparison of the 5- and 9-in DA4002 at $Re = 28,7000$ from PROPID: (a) thrust coefficient, (b) power coefficient, and (c) efficiency.

c/R values and that is seen as a slightly larger thrust and power coefficient values. Also seen in Fig. 38 is the effect of the Reynolds number. While the power coefficient changes very little for most of the propellers, there is a clear increase in the thrust coefficient as the Reynolds number increases. From Eq. 13, the increase in thrust is most likely due to an increase in the lift coefficient along the blade. Since the power coefficient is not increasing, a decrease in drag is probably also occurring (Eq. 14).

A different Reynolds number effect is seen in the static results of the GWS 5×4.3 propeller (Fig. 39). As the Reynolds number increases, the thrust coefficient stays about the same while the power coefficient decreases. These results show that the drag decrease along the propeller blade is more dominate than any lift increase.

The static results of the Micro Invent 5×3.5 (Fig. 40) are discussed to demonstrate a problem that can occur for small propellers with thin blades. As seen in the static results, both the thrust and power coefficients increase with the Reynolds number, so it might be concluded that the lift increase along the blade overcomes any drag decrease. However, noticeable bending was seen in the propeller during testing. From the APC static results shown in Fig. 38, an increase in the pitch will increase both the thrust and power coefficients, so it is possible that while the Micro Invent propeller was bending, it was also twisting to create

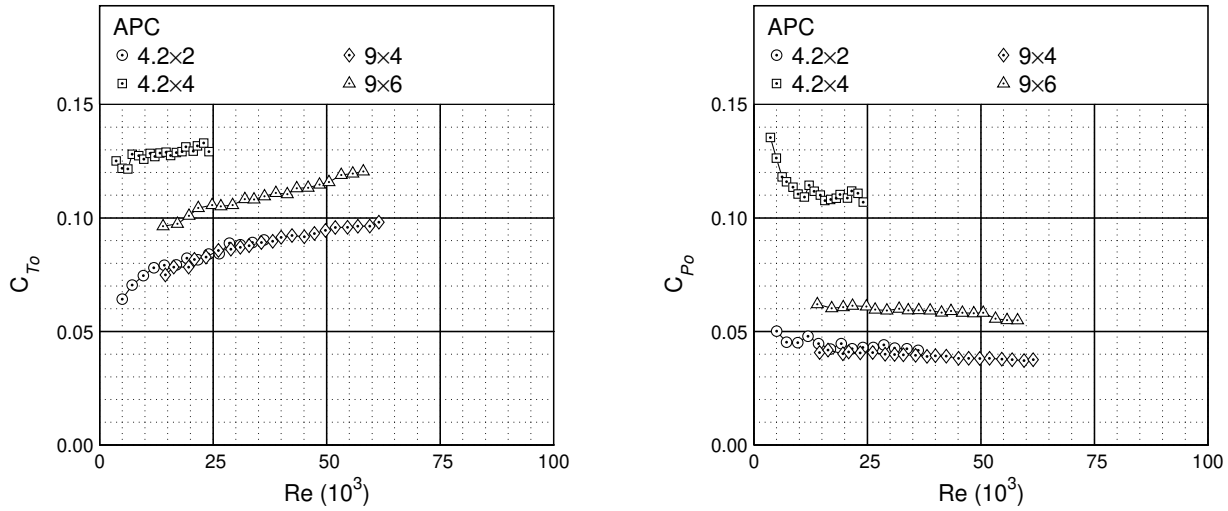

(a) (b)

Figure 38: Static performance of the APC propellers as a function of Reynolds number: (a) C_{T_0} data and (b) C_{P_0} data.

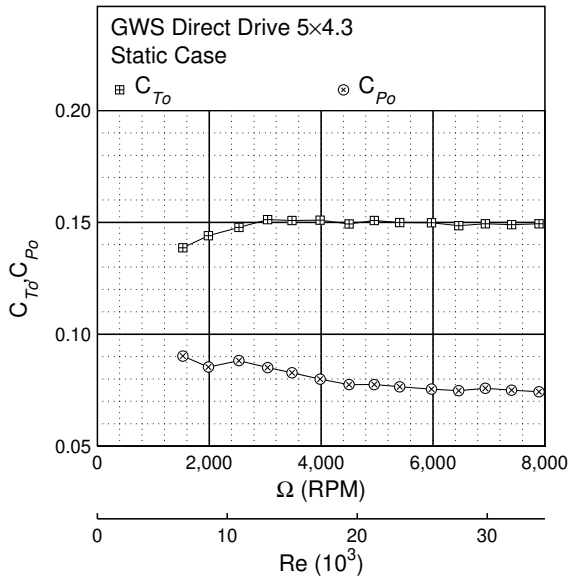

Figure 39: GWS Direct Drive 5×4.3 static performance.

a larger pitch. To determine if twisting occurred, photographs of the propeller were taken using a strobe light and digital camera while it was spinning. From the side views in Fig. 41, it is seen that the propeller is deforming under load. Using PropellerScanner, the geometry of the propeller was measured while it was under load, and those results are shown in Fig. 42. A clear increase in the pitch of the propeller is shown. While Reynolds number effects could be present for the Micro Invent propeller, the change in the propeller pitch is most likely the dominate reason for the thrust and power increase seen in the static performance results.

Results for the 3D printed DA4002 propeller are shown in Fig. 43, and Reynolds number effects are seen in both the thrust and power coefficients. As the Reynolds number increases, the thrust coefficient increases and the drag coefficient decreases. It is also seen that there is good agreement between the 5- and 9-in

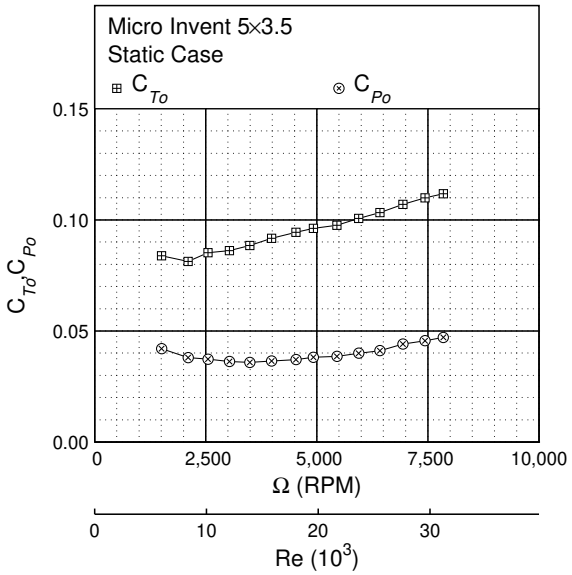

Figure 40: Micro Invent 5×3.5 static performance.

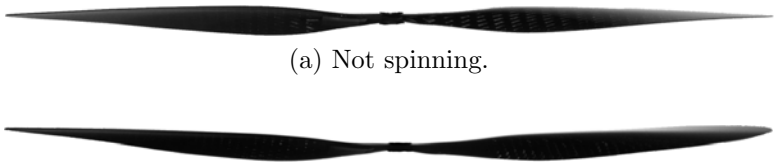

(a) Not spinning.

(b) 7,000 RPM.

Figure 41: Micro Invent 5×3.5 propeller under static conditions (thrust is pointed up).

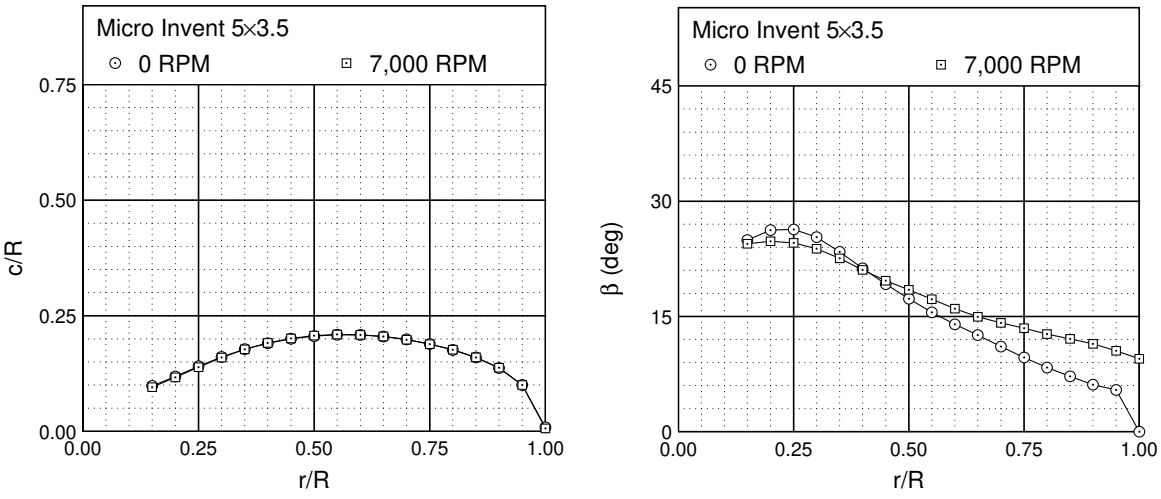

(a) (b)

Figure 42: Geometry comparison of the Micro Invent 5×3.5 propeller while at rest and at 7,000 RPM during static conditions: (a) chord distribution and (b) twist distribution.

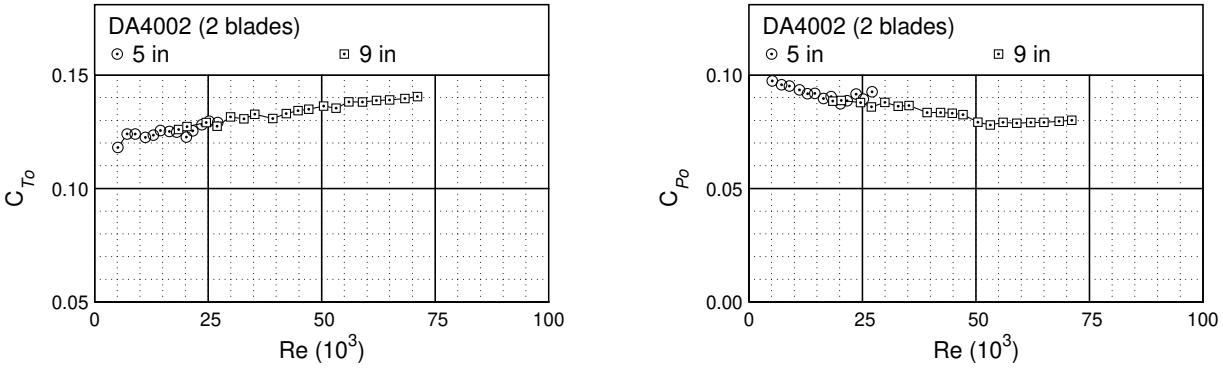

(a) (b)

Figure 43: Static performance comparison for the 2-blade DA4002: (a) thrust coefficient and (b) power coefficient.

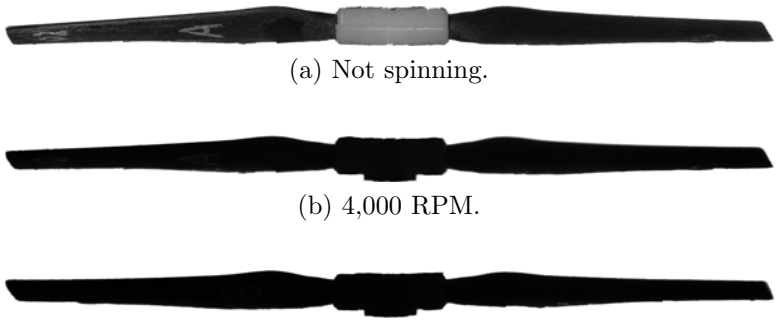

(a) Not spinning.

(b) 4,000 RPM.

(c) 6,000 RPM.

Figure 44: The 5-in DA4002 under static conditions (thrust is pointed up).

propellers when they are at the same Reynolds number. The increase in the thrust coefficient and decrease in the power coefficient correspond to an increase in the lift coefficient and a decrease in the drag coefficient along the propeller blade. The static performance results of these scaled propellers can be used to predict the performance of other propellers with different diameters but operating at the same Reynolds numbers.

While some bending was observed during the testing of the DA4002 propellers, it was predicted that the propellers were not twisting since the power coefficient was not increasing as was the case with the Micro Invent propeller. To determine if this prediction was correct, photographs of both the 5- and 9-in propellers were taken while they were spinning. The side view photographs of the propellers are shown in Figs. 44 and 45, and the PropellerScanner results are shown in Figs. 46 and 47. While the photographs show that there is some bending, the PropellerScanner results show that propellers are not twisting, so the changes in the thrust and power coefficients from Fig. 43 are due to Reynolds number effects and not to any change in propeller geometry.

A comparison between the 5- and 9-in NR640 propellers is shown in Fig. 48. The results between the two propellers do not match like the two DA4002 propellers, but as discussed earlier in Section III, the geometry of the two NR640 propellers were not identical due to manufacturing problems. Both propellers do, however, show similar Reynolds number effects. As the Reynolds number increases, the thrust coefficient increases and the power coefficient stays about the same. The 5-in propeller also sees a decrease in the power coefficient at the lowest Reynolds numbers.

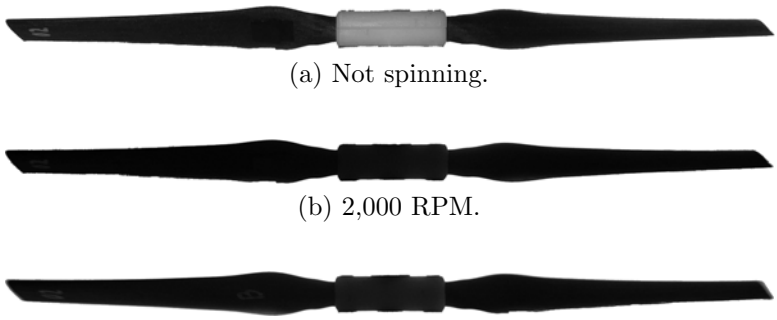

(a) Not spinning.

(b) 2,000 RPM.

(c) 3,000 RPM.

Figure 45: The 9-in DA4002 under static conditions (thrust is pointed up).

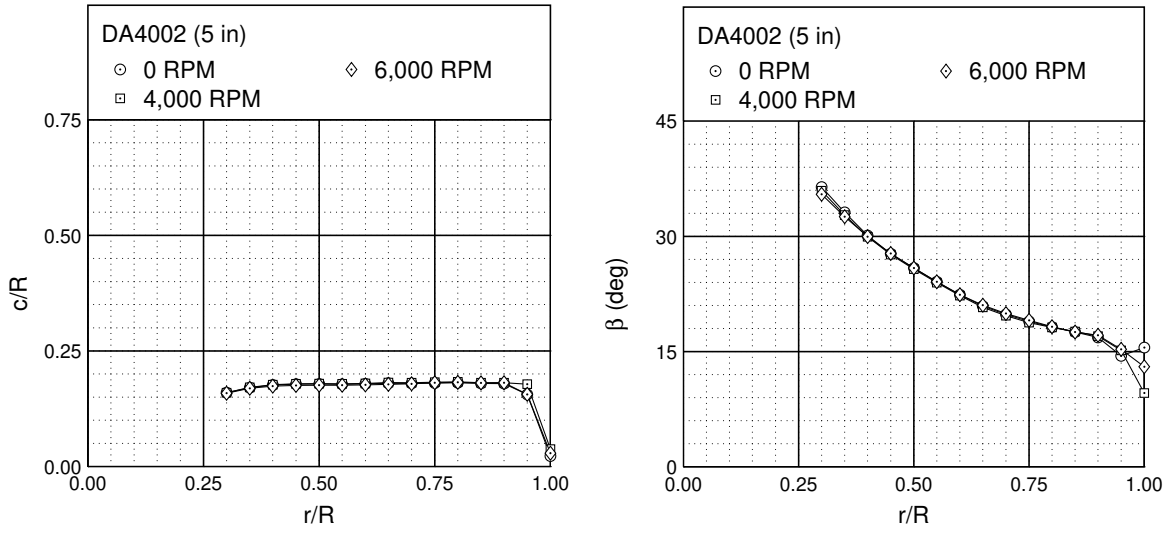

(a) (b)

Figure 46: Geometry comparison of the 5-in DA4002 while at rest, 4,000 RPM, and 6,000 RPM during static conditions: (a) chord distribution and (b) twist distribution.

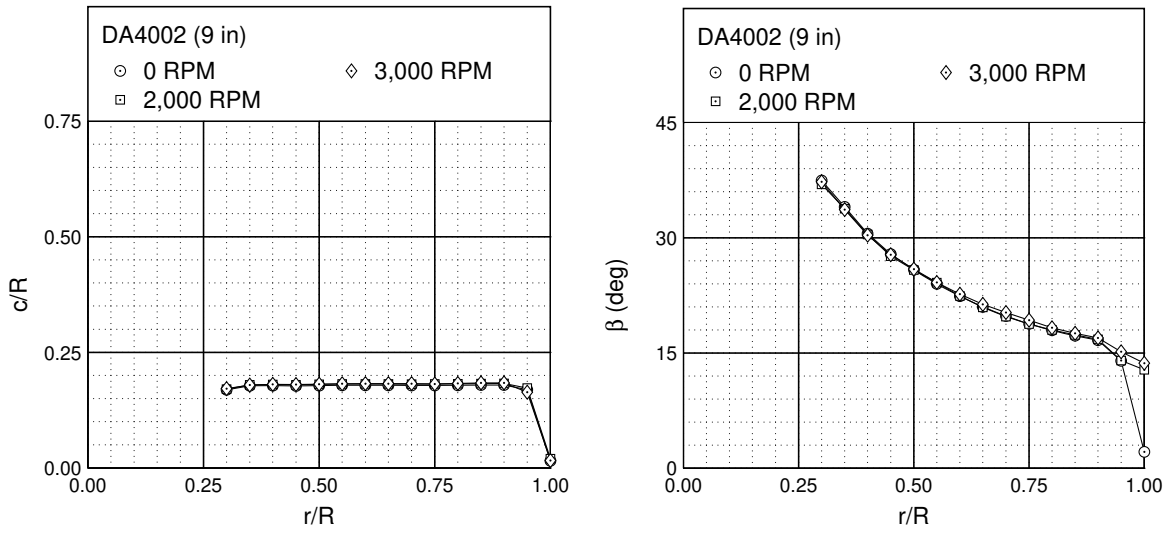

(a) (b)

Figure 47: Geometry comparison of the 9-in DA4002 while at rest, 2,000 RPM, and 3,000 RPM during static conditions: (a) chord distribution and (b) twist distribution.

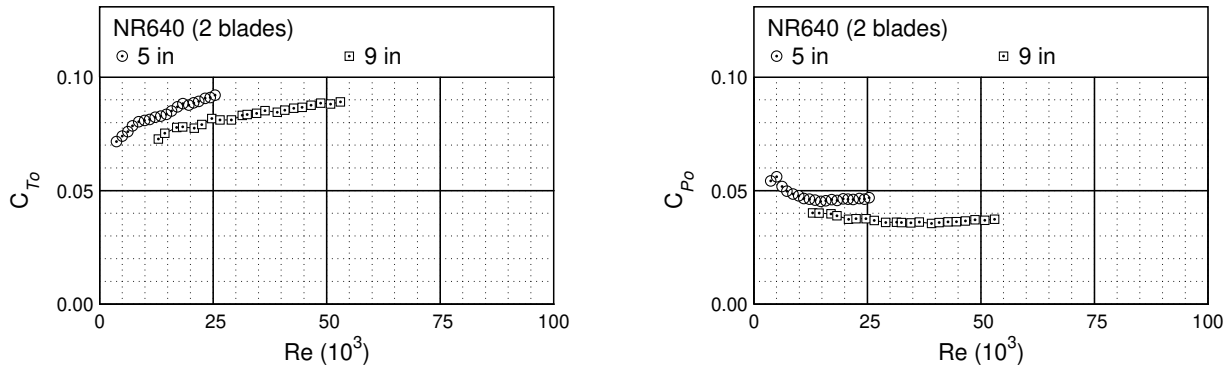

(a) (b)

Figure 48: Static performance comparison for the 2-blade NR640: (a) thrust coefficient and (b) power coefficient.

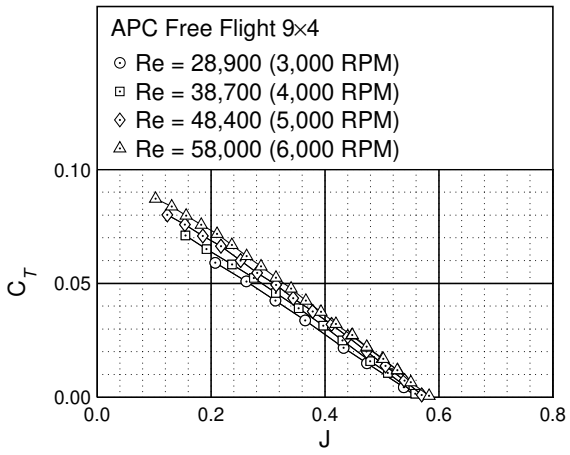

Figure 49: APC Free Flight 9×4 thrust coefficient.

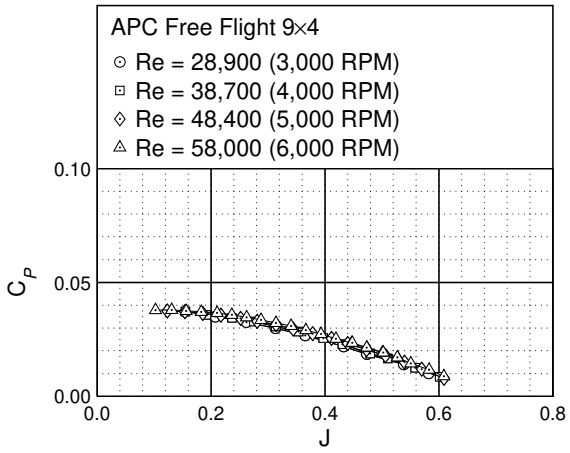

Figure 50: APC Free Flight 9×4 power coefficient.

B. Advancing-Flow Tests

Results for the APC 9×4 propeller in an advancing flow are shown in Figs. 49–51. As was seen in the static performance results (Fig. 38), the thrust coefficient increases with the Reynolds number, but no large change is visible with the power coefficient. The thrust coefficient increase leads to an increase in the propeller efficiency as shown in Fig. 51. Similar to the static results, the Reynolds number effects for the GWS 5×4.3 propeller are different than the APC 9×4. As the Reynolds number increases, the thrust coefficient (Fig. 52) does not change while the power coefficient (Fig. 53) decreases. An increase in the efficiency (Fig. 54) with an increase in the Reynolds number is still measured with this propeller. From these two propellers, it is clear that as the Reynolds number increases, an increase in the thrust coefficient, a decrease in the power coefficient, or both will increase the propeller efficiency. For the APC propeller, the maximum efficiency increased from about 45% to 55%, and the maximum efficiency for the GWS propeller increased from about 62% to 66%.

Figures 55–57 show the results of the Micro Invent 5×3.5 propeller. It was shown earlier that this propeller deformed during static testing, and the advancing-flow results also show this geometry change. The largest difference in the behavior of the Micro Invent propeller to the APC and GWS propellers is seen in the power coefficient (Fig. 56). At the two larger rotation rates, the power coefficient did not continue

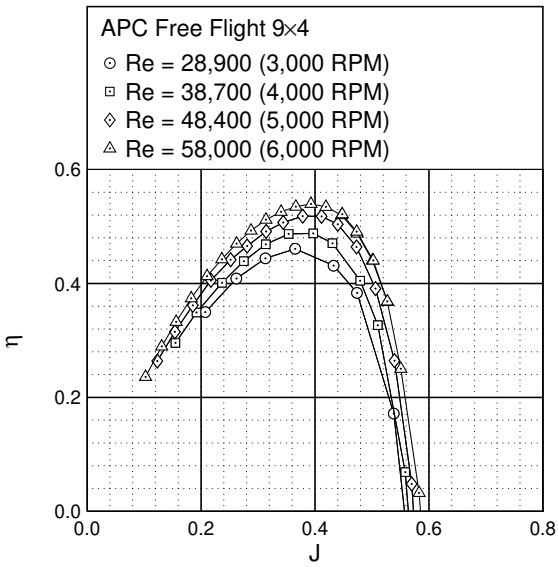

Figure 51: APC Free Flight 9×4 efficiency curves.

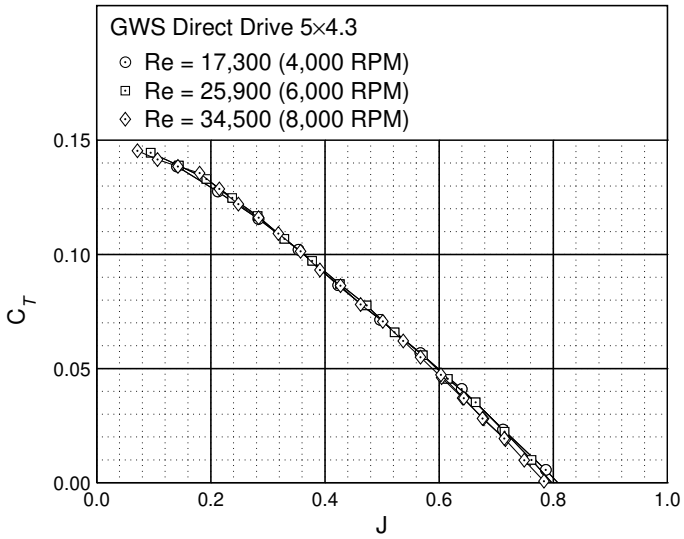

Figure 52: GWS Direct Drive 5×4.3 thrust coefficient.

towards zero as the advance ratio increased, but instead it started to increase. It is believed that as the advance ratio increased past the point of zero thrust, the propeller continued to deform.

The advancing-flow results of the 9-in DA4002 propeller are shown in Figs. 58–60. A clear increase in the thrust coefficient is seen along with a decrease in the power coefficient at lower advance ratios as the Reynolds number increases. Overall the efficiency of the propeller increases with the Reynolds number. The Reynolds number effects seen in these results are similar to the effects seen in the PROPID results from Section IV. The 5- and 9-in propellers were both tested at approximately the same Reynolds number, and Fig. 61 shows that the results are very close as expected.

Performance data of the 9-in NR640 propeller are compared to the full-scale tests[28] in Figs. 62–64. The 9-in propeller shows the effect of increasing the Reynolds number as an increase in the thrust coefficient. Thrust and power coefficient values for the 9-in propeller are lower than the 10-ft propeller though the

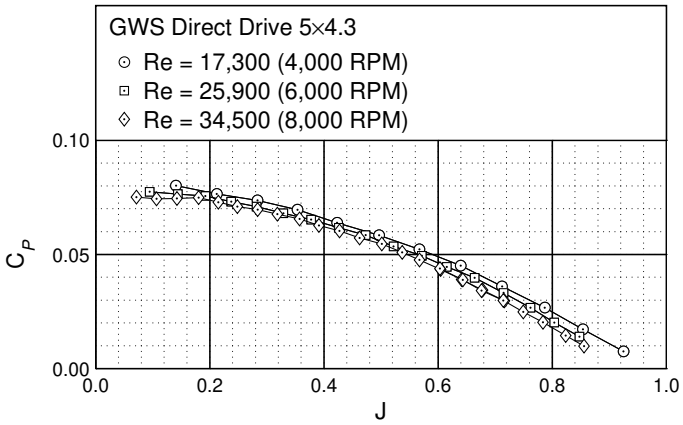

Figure 53: GWS Direct Drive 5×4.3 power coefficient.

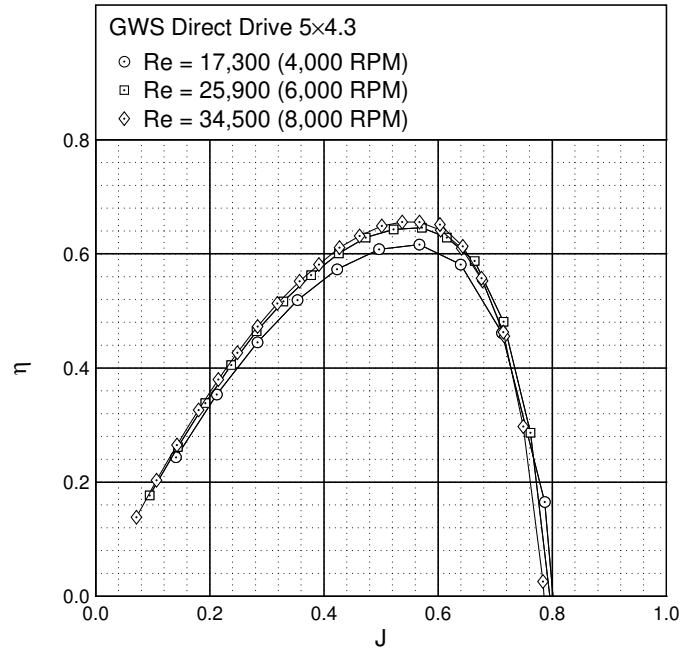

Figure 54: GWS Direct Drive 5×4.3 efficiency curves.

difference in the thrust coefficient is significantly more than the difference in the power coefficient. In fact at the lower advance ratios, the power coefficient between the two propellers is very close. While the 9-in propeller tested in this research was not an exact match to the desired geometry (Fig. 27), the difference in geometry is small and would not account for all of the differences seen in the performance. The full-scale propeller was tested at a much larger Reynolds number, so the lift coefficient is expected to be larger and the drag coefficient is expected to be smaller than those of the 9-in propeller. The size and speed of the propeller also places part of 10-ft propeller blade beyond the incompressible limit of Mach 0.3. The tip Mach number for the full-scale propeller is around 0.56. These Reynolds number and Mach number differences explain the large differences in the thrust coefficient between the 9-in and 10-ft propellers, and this difference in also seen in the efficiency curves. While the 10-ft propeller reaches a maximum efficiency of just over 80%, the maximum efficiency of the 9-in propeller is below 65%.

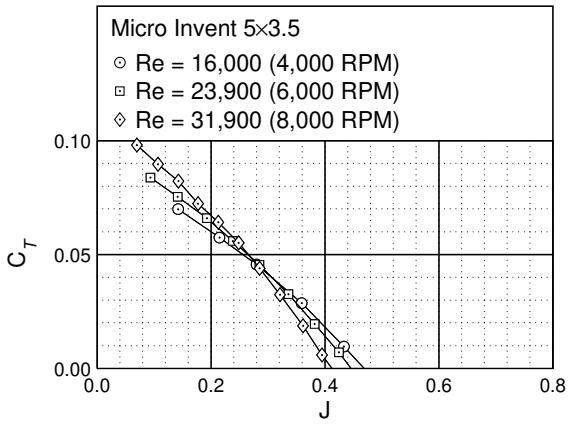

Figure 55: Micro Invent 5×3.5 thrust coefficient.

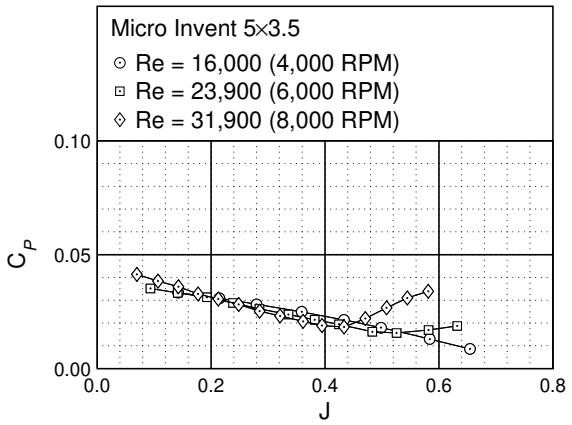

Figure 56: Micro Invent 5×3.5 power coefficient.

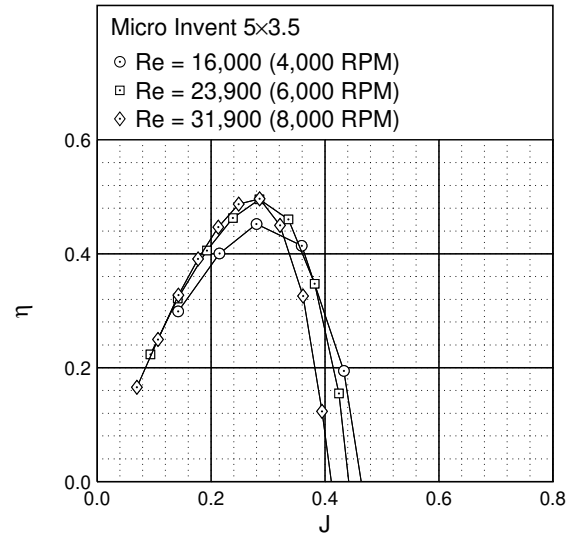

Figure 57: Micro Invent 5×3.5 efficiency curves.

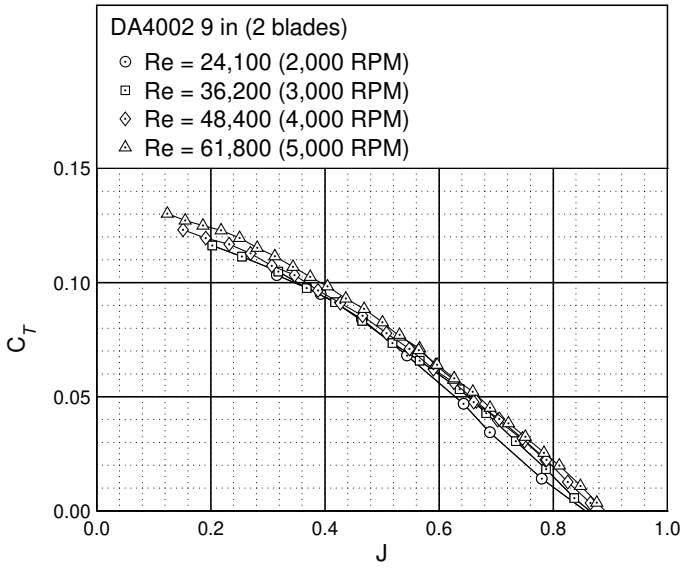

Figure 58: DA4002 9×6.75 thrust coefficient.

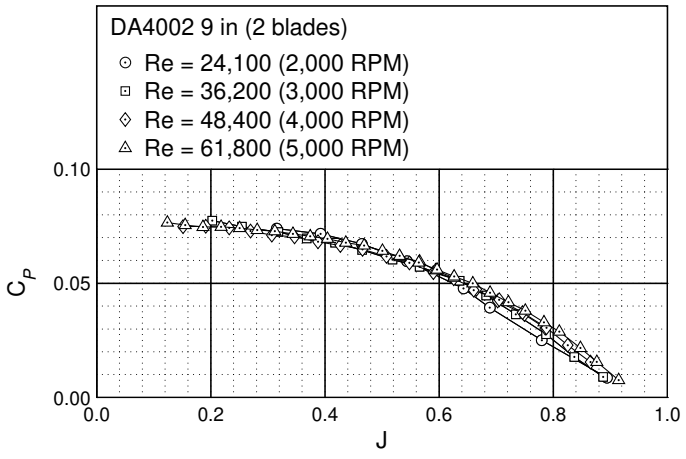

Figure 59: DA4002 9×6.75 power coefficient.

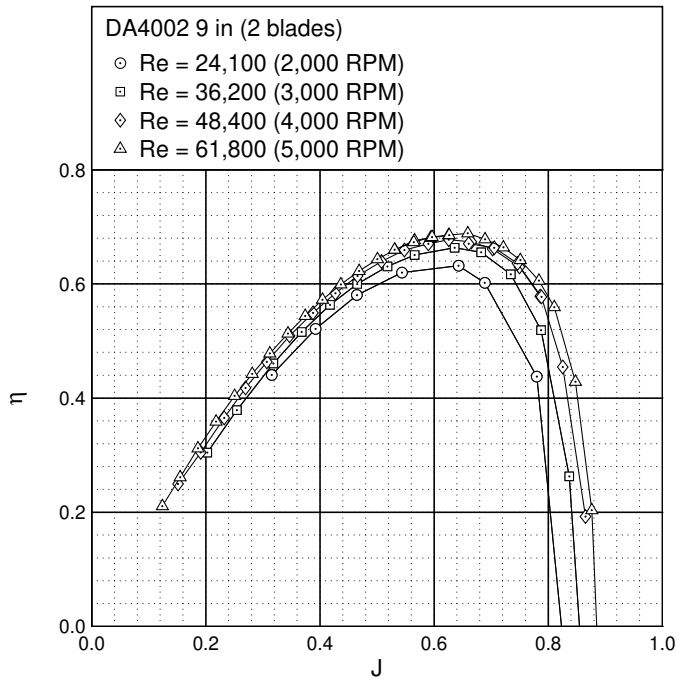

Figure 60: DA4002 9×6.75 efficiency curves.

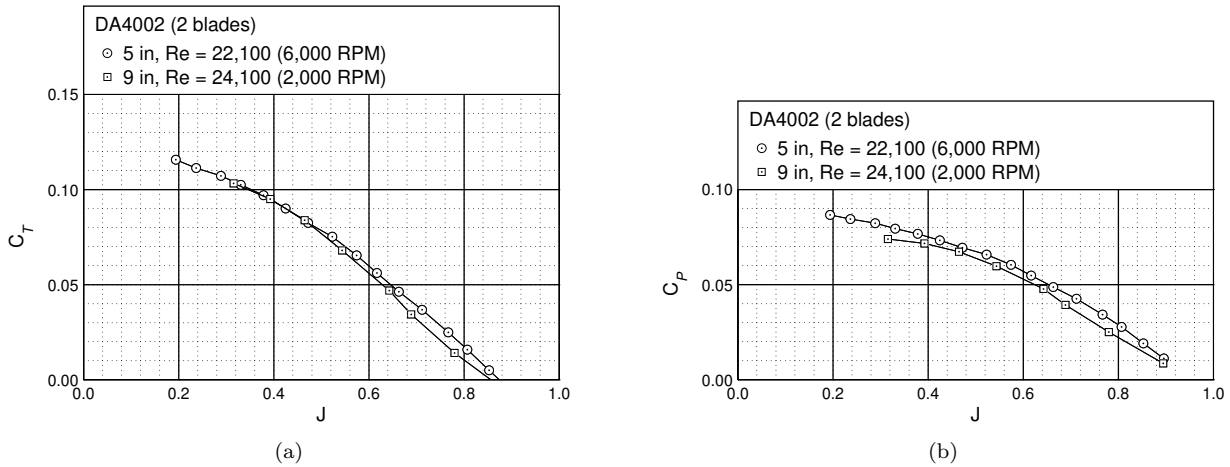

(a) (b)

Figure 61: Performance comparison for the 2-blade DA4002: (a) thrust coefficient and (b) power coefficient.

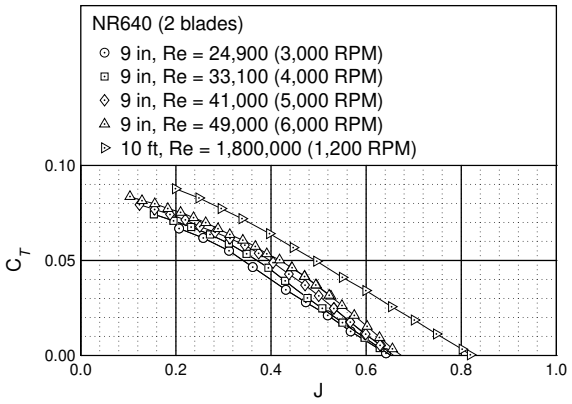

Figure 62: Thrust coefficient for the 2-blade NR640 (10-ft propeller data from NACA Report 640[28]).

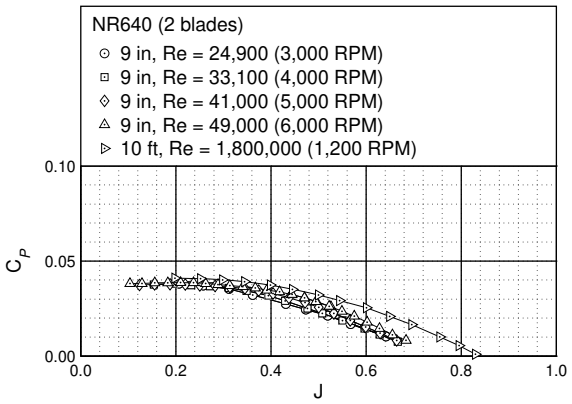

Figure 63: Power coefficient for the 2-blade NR640 (10-ft propeller data from NACA Report 640[28]).

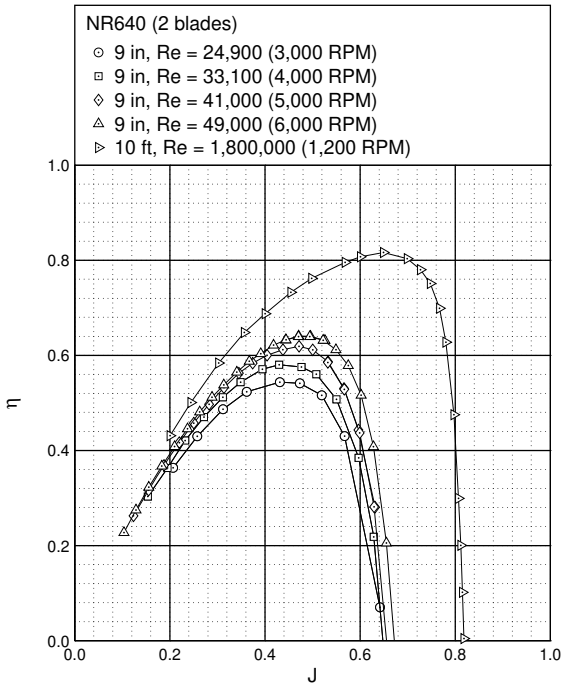

Figure 64: Efficiency curves for the 2-blade NR640 (10-ft propeller data from NACA Report 640[28]).

VI. Conclusions

The small-scale nature of propellers used for small UAVs and MAVs lead to difficulty in predicting their behavior. Part of this difficulty is from the large dependence the performance has on the propeller Reynolds number. To help measure this Reynolds number dependence, static and advancing-flow performance data were measured for a variety of off-the-shelf and 3D-printed propellers. From these tests, the main Reynolds number effects have been confirmed. As the Reynolds number increases, the thrust coefficient increases, the power coefficient decreases, or both. The changes in the thrust and power coefficients are due to the increase in the sectional lift coefficients and the decrease in the sectional drag coefficients with increasing Reynolds numbers, which are typical in this Reynolds number range. For propellers in an advancing flow, the Reynolds number effects lead to an increase in the propeller efficiency, and as shown with the APC 9×4, this increase can be at least 10%. Nevertheless, the maximum efficiency of these propellers is still low when compared to the efficiency of a full scale propeller as was shown with the NR640 propeller.

While the off-the-shelf propellers were useful in measuring the general Reynolds number trends, they were limiting in the geometry available. The 3D-printed propellers developed for this researched showed that propellers of different diameters will have the same performance coefficients when they operate at the same Reynolds number. With this behavior, the performance of a new propeller with a different diameter can be predicted based on the known performance of a propeller; the new propeller will have the same performance when it operates in the Reynolds number range of the known propeller. If the new propeller also operates at larger Reynolds numbers, it is expected that its efficiency will increase; however, its efficiency will decrease at lower Reynolds numbers.

Acknowledgments

The authors would like to thank Matthew Dempsey and Rushant Badani for their help in taking propeller wind tunnel data.

A. Airfoil Coordinates

Table 3: SDA1045 coordinates

x/c	y/c	x/c	y/c
1.000070	0.002873	0.000286	−0.001933
0.996513	0.003274	0.004737	−0.007900
0.986303	0.004659	0.015121	−0.014214
0.970118	0.006938	0.030392	−0.020215
0.948330	0.009944	0.050469	−0.025633
0.921215	0.013609	0.075197	−0.030334
0.889158	0.018020	0.104397	−0.034211
0.852698	0.023151	0.137836	−0.037224
0.812409	0.028921	0.175231	−0.039349
0.768902	0.035210	0.216249	−0.040604
0.722815	0.041851	0.260503	−0.041020
0.674815	0.048625	0.307565	−0.040655
0.625484	0.055198	0.356962	−0.039581
0.575326	0.061337	0.408182	−0.037887
0.524859	0.066841	0.460684	−0.035673
0.474592	0.071531	0.513900	−0.033051
0.425015	0.075227	0.567248	−0.030145
0.376590	0.077790	0.620100	−0.027119
0.329754	0.079095	0.671787	−0.024087
0.284903	0.079060	0.721652	−0.021131
0.242412	0.077625	0.769059	−0.018321
0.202604	0.074778	0.813395	−0.015705
0.165777	0.070531	0.854082	−0.013315
0.132169	0.064953	0.890581	−0.011162
0.102002	0.058163	0.922400	−0.009240
0.075442	0.050321	0.949090	−0.007508
0.052653	0.041670	0.970384	−0.005805
0.033778	0.032467	0.986225	−0.004219
0.018955	0.023025	0.996352	−0.003158
0.008278	0.013710	0.999923	−0.002872
0.001884	0.005012		

Table 4: SDA1075 coordinates

x/c	y/c	x/c	y/c
1.000137	0.005557	0.000280	−0.001921
0.996593	0.005916	0.004701	−0.007905
0.986424	0.007201	0.015056	−0.014217
0.970307	0.009369	0.030301	−0.020208
0.948605	0.012241	0.050355	−0.025609
0.921585	0.015743	0.075069	−0.030290
0.889621	0.019963	0.104265	−0.034146
0.853243	0.024878	0.137711	−0.037140
0.813012	0.030409	0.175126	−0.039253
0.769531	0.036448	0.216177	−0.040503
0.723430	0.042837	0.260479	−0.040926
0.675369	0.049377	0.307602	−0.040585
0.625945	0.055764	0.357073	−0.039554
0.575694	0.061768	0.408381	−0.037928
0.525145	0.067169	0.460985	−0.035812
0.474806	0.071778	0.514304	−0.033341
0.425168	0.075411	0.567727	−0.030638
0.376692	0.077929	0.620617	−0.027832
0.329814	0.079200	0.672308	−0.025029
0.284932	0.079143	0.722150	−0.022300
0.242417	0.077694	0.769510	−0.019711
0.202594	0.074839	0.813783	−0.017302
0.165758	0.070588	0.854396	−0.015105
0.132147	0.065010	0.890816	−0.013128
0.101982	0.058221	0.922559	−0.011366
0.075425	0.050381	0.949178	−0.009777
0.052643	0.041731	0.970411	−0.008207
0.033775	0.032527	0.986204	−0.006742
0.018960	0.023081	0.996295	−0.005793
0.008287	0.013758	0.999851	−0.005553
0.001894	0.005047		

Table 5: SDA1100 coordinates

x/c	y/c	x/c	y/c
1.000560	0.023438	0.000340	−0.002210
0.997176	0.023296	0.004895	−0.008428
0.987335	0.023394	0.015242	−0.014980
0.971591	0.024273	0.030432	−0.021172
0.950250	0.025737	0.050398	−0.026752
0.923550	0.027790	0.075000	−0.031600
0.891891	0.030470	0.104069	−0.035622
0.855748	0.033756	0.137381	−0.038791
0.815637	0.037595	0.174659	−0.041092
0.772117	0.041913	0.215573	−0.042554
0.725782	0.046610	0.259744	−0.043220
0.677260	0.051562	0.306745	−0.043157
0.627196	0.056606	0.356104	−0.042445
0.576247	0.061546	0.407313	−0.041185
0.525001	0.066102	0.459831	−0.039483
0.473983	0.070072	0.513086	−0.037462
0.423703	0.073265	0.566488	−0.035252
0.374641	0.075528	0.619404	−0.033012
0.327253	0.076718	0.671164	−0.030854
0.281953	0.076738	0.721110	−0.028861
0.239131	0.075504	0.768602	−0.027101
0.199125	0.072979	0.813026	−0.025615
0.162245	0.069148	0.853802	−0.024436
0.128746	0.064047	0.890388	−0.023569
0.098854	0.057737	0.922293	−0.023005
0.072735	0.050335	0.949072	−0.022707
0.050524	0.041973	0.970376	−0.022572
0.032250	0.032866	0.986071	−0.022580
0.017968	0.023382	0.995899	−0.023006
0.007743	0.013912	0.999280	−0.023331
0.001686	0.004982		

References

[1]Carmichael, B. H., "Low Reynolds Number Airfoil Survey," NASA CR 165803, 1981.

[2]Selig, M. S., Donovan, J. F., and Fraser, D. B.,, *Airfoils at Low-Speeds*, SoarTech Publications, Virginia Beach, VA, 1989.

[3]Selig, M. S., Guglielmo, J. J. A. P. Broeren, A. P., and Giguère, P., *Summary of Low-Speed Airfoil Data*, Vol. 1, SoarTech Publications, Virginia Beach, VA, 1995.

[4]Selig, M. S., Lyon, C. A., Giguère, P., Ninham, C. P., and Guglielmo, J. J., *Summary of Low-Speed Airfoil Data*, Vol. 2, SoarTech Publications, Virginia Beach, VA, 1996.

[5]Lyon, C. A., Broeren, A. P., Giguère, P., Gopalarathnam, A., and Selig, M. S., *Summary of Low-Speed Airfoil Data*, Vol. 3, SoarTech Publications, Virginia Beach, VA, 1998.

[6]Selig, M. S., and McGranahan, B. D., "Wind Tunnel Aerodynamic Tests of Six Airfoils for Use on Small Wind Turbines," National Renewable Energy Laboratory, NREL/SR-500-34515, Golden, CO, 2004.

[7]Williamson, G. A., McGranahan, B. D., Broughton, B. A., Deters, R.W ., Brandt, J. B., and Selig, M. S., *Summary of Low-Speed Airfoil Data*, Vol. 5, 2012.

[8]Borst, H. V. and Associates, "Aerodynamic Design and Analysis of Propellers for Mini-Remotely Piloted Air Vehicles: Volume 1 — Open Propellers," USAAMRDL-TR-77-45A, 1978.

[9]Bass, R. M., "Small Scale Wind Tunnel Testing of Model Propellers," AIAA Paper 86-0392, 1986.

[10]Ol, M., Zeune, C., and Logan M., "Analytical-Experimental Comparison for Small Electric Unmanned Air Vehicle Propellers," AIAA Paper 2008-7345, 2008.

[11]Moffitt, B. A., Bradley, T. H., Parekh, D. E., and Mavris, D., "Validation of Vortex Propeller Theory for UAV Design with Uncertainty Analysis," AIAA Paper 2008-0406, 2008.

[12]Brandt, J. B., "Small-Scale Propeller Performance at Low Speeds," M.S. Thesis, University of Illinois at Urbana-Champaign, Urbana, IL, 2005.

[13]Uhlig, D. V., "Post Stall Propeller Behavior at Low Reynolds Numbers," M.S. Thesis, University of Illinois at Urbana-Champaign, Urbana, IL, 2007.

[14]Merchant, M. P. and Miller, L. S., "Propeller Performance Measurement for Low Reynolds Number UAV Applications," AIAA Paper 2006-1127, 2006.

[15]Gamble, D. E. and Arena, A., "Automated Dynamic Propeller Testing at Low Reynolds Numbers," AIAA Paper 2010-0853, 2010.

[16]Baranski, J. A., Fernelius, M. H., Hoke, J. L., Wilson, C. W., and Litke, P. J., "Characterization of Propeller Performance and Engine Mission Matching for Small Remotely Piloted Aircraft," AIAA Paper 2011-6058, 2011.

[17]Brandt, J. B. and Selig, M. S., "Propeller Performance Data at Low Reynolds Numbers," AIAA Paper 2011-1255, 2011.

[18]Deters, R. W. and Selig, M. S., "Static Testing of Micro Propellers," AIAA Paper 2008-6246, 2008.

[19]Deters, R. W., "Performance and Slipstream Characteristics of Small-Scale Propellers at Low Reynolds Numbers," Ph.D. Dissertation, University of Illinois at Urbana-Champaign, Urbana, IL, 2014.

[20]Smedresman, A., Yeo, D., and Shyy, W., "Design, Fabrication, Analysis, and Testing of a Micro Air Vehicle Propeller," AIAA Paper 2011-3817, 2011.

[21]Khodadoust, A., "An Experimental Study of the Flowfield on a Semispan Rectangular Wing with a Simulated Glaze Ice Accretion," Ph.D. Dissertation, University of Illinois at Urbana-Champaign, Urbana, IL, 1993.

[22]Anderson, J. D., Jr., *Fundamentals of Aerodynamics*, 2nd ed., McGraw-Hill, Inc., New York, 1991.

[23]Glauert, H., "Wind Tunnel Interference on Wings, Bodies and Airscrews," Aeronautical Research Committee R&M 1566, 1933.

[24]Barlow, J. B., Rae, W. H., Jr., and Pope, A., *Low-Speed Wind Tunnel Testing*, 3rd ed., John Wiley & Sons, Inc., New York, 1999.

[25]Hepperle, M., PropellerScanner, http://mh-aerotools.de, Accessed May 27, 2014.

[26]Uhlig, D. V. and Selig, M. S., "Post Stall Propeller Behavior at Low Reynolds Numbers," AIAA Paper 2008-0407, 2008.

[27]Selig, M. S., UIUC Applied Aerodynamics Group, http://aerospace.illinois.edu/m-selig/, Accessed May 27, 2014.

[28]Hartman, E. P. and Biermann, D., "The Aerodynamic Characteristics of Full-Scale Propellers Having 2, 3, and 4 Blades of Clark Y and R.A.F. 6 Airfoil Sections," NACA Report 640, 1938.

[29]Drela, M., XFOIL, http://web.mit.edu/drela/Public/web/xfoil/, Accessed May 27, 2014.

[30]Selig, M. S. and Tangler, J. L., "Development and Application of a Multipoint Inverse Design Method for Horizontal Axis Wind Turbines," *Wind Engineering*, Vol. 19, No. 2, 1995, pp. 91.

[31]Selig, M. S. and Maughmer, M. D., "Multipoint Inverse Airfoil Design Method Based on Conformal Mapping," *AIAA Journal*, Vol. 30, No. 5, May 1992, pp. 1162–1170.

[32]Selig, M. S. and Maughmer, M. D., "Generalized Multipoint Inverse Airfoil Design," *AIAA Journal*, Vol. 30, No. 11, November 1992, pp. 2618–2625.

[33]Johnson, W., *Helicopter Theory*, Dover Publications, Inc., New York, 1980.

[34]Leishman, J. G., *Principles of Helicopter Aerodynamics*, Cambridge University Press, Cambridge, 2000.

[35]McCormick, B. W., *Aerodynamics, Aeronautics, and Flight Mechanics*, John Wiley and Sons, Inc, New York, 1995.

[36]McGranahan, B. D., "Surface Oil Flow Measurements on Several Airfoils at Low Reynolds Numbers," M.S. Thesis, University of Illinois at Urbana-Champaign, Urbana, IL, 2003.